GRAVITATIONAL LENSING WITH MULTIPLE SOURCES

constraining cosmology and lens properties using time delays

A Master Thesis in Cosmology

Christoffer Sunesson

2004

Department of Astronomy, Stockholm University

Gravitational Lensing with Multiple Sources
constraining cosmology and lens properties using time delays

Christoffer Sunesson

December 2004

Abstract

The possibility to use time delays from gravitationally lensed multiple sources to estimate the logarithmic slope of the density parameter η, the matter energy density parameter Ω_M and the Hubble constant H_0 in a flat universe is investigated.

By using the flux ratios, η can be estimated. It is found to depend on the differences between the image angles and on the uncertainty in the observed flux ratio.

By using the quotient between the time delays, Ω_M can be estimated. It is found to depend on the angular distances between the sources, on the image angle separations and on the uncertainties in the image angles and in the time delays.

By combining the time delays, H_0 can be estimated, and is found to depend mainly on η and the angular distance to the lens.

Contents

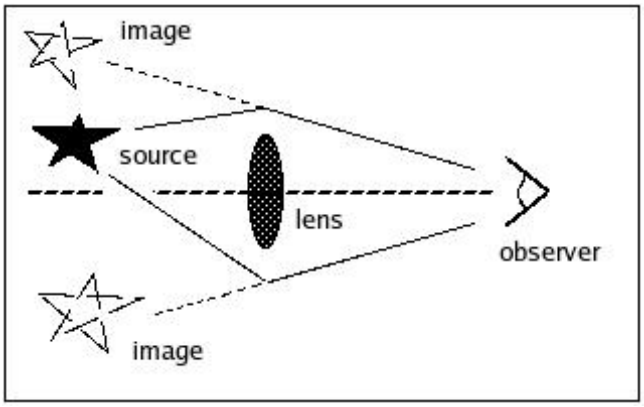

Figure 1: Gravitational lensing occurs when a massive object is acting as a lens on a background object, light rays that would have otherwise not reached us are bent from their path and the source appears in another position.

Introduction

This thesis is the final part toward a master degree in physics at the Department of Physics/Astronomy at Stockholm University, under supervision of Edvard Mörtsell.

The quest for the cosmological parameters that determines the geometry, the history and the dynamics of the universe is a long-standing issue in observational cosmology. By combining observations from e.g. the Cosmic Microwave Background and the luminosity from distant type Ia supernovae, a new standard model of cosmology has emerged; a flat universe with an accelerating expansion.

A method to obtain information about the large-scale geometry of the universe is through *gravitational lensing*, see Fig. (1). Since the effects from gravitational lensing depends on the ratio of the angular size distances which are sensitive to the cosmological parameters, investigations of a gravitationally lensed system can reveal information about the cosmology.

In this thesis I investigate how some of the cosmological parameters can be estimated through time delays from a gravitationally lensed system where two sources are multiple lensed, i.e. when two or more images from one source appears. I call a system where four images appears from two sources (two from each), that is two families of two images [10], for a *Double Objects Lensing*[1] system, abbreviated as DOL. In all simulations I assume we are living in a flat universe.

[1] I have not found any good name for this kind of system, so the name *Double Objects Lensing* is something I have made up myself.

This thesis is split into seven parts:

Chapter 1 very briefly introduces gravitation, the electromagnetic force and optics.

Chapter 2 is about cosmology and introduces, explains and derives the cosmological parameters that I estimate through DOL.

Chapter 3 explains gravitational lensing and how important the role of the lens is. Two lens models are explained and in each one a time delay function is derived; the most important equations in my DOL-simulations.

Chapter 4 deals with double objects lensing and explains how the DOL-systems are simulated, the statistical tools that are used, how the cosmological parameter estimations depend on the measurable parameters, how the flux ratio can be used to estimate the halo profile of the lens and discusses the uncertainties that appears.

Chapter 5 presents the results from my simulations. I simulate five DOL-system with different observables and investigates how different DOL-systems affects the estimations. Two types of estimations are made for each simulation, one where the time delay quotient is used and another where the time delays are summed.

Chapter 6 discuss the results from the simulations and prospects for the future of using time delays from DOL-systems.

Appendix contains some tricky or too long calculation that had to be made but does not fit inside the thesis.

1 The Nature of Gravity and Light

1.1 Gravitation

In our everyday life we are all affected by the natural force of gravity, sometimes it does us good and sometimes it pains, like when one is jogging upward in a terrain trail. For many people gravity is associated with Newton, hit by an apple while sitting under a tree. However, what Newton really wanted to show with the story of the falling apple, was a phenomena that happens between all bodies everywhere in the universe. Newton had found, that the phenomena of gravity that pulls the apple down is acting on every massive object in the universe. So likewise, the falling apple could be the earth and the ground could be the sun, lucky for us the earth's velocity around the sun saves us from crashing into it.

The gravity one feels from an object is due to its mass and ones own mass, the more massive object you interact with, the more the force of gravity tugs on you. The gravitational force between two object's is attractive and central, i.e. along the line of centers of mass. The universal law of gravity that Newton found was

$$F_{gravity} = -\frac{G\,M_a\,M_b}{R^2}\,\hat{\mathbf{R}}_{ab} \tag{1}$$

where G is the gravitational constant[2] which has the same value for all materials, for this reason the law is called the universal law of gravitation. M_a and M_b are the masses of the objects, R is the distance and the vector $\hat{\mathbf{R}}_{ab}$ denotes the direction of the force from the object exerting the force, in this case from object a, to the object experiencing the force, object b.

1.2 The Electromagnetic Force

Another force of nature that we witness in our daily life is the electromagnetic force, the force that gives us light in all its shapes[3]. Like the force of gravity is interacting between all objects with mass, the electromagnetic force is interacting with all objects with charge, with one difference; the electromagnetic force can both be attractive and repulsive. The charge of an object can be positive or negative. Similar to an object with mass, an object with charge builds up a force field stretching out in every direction from it. The electrostatic force between different charges is called Coulomb's law and it is given by

$$F_{coulomb} = k_E\frac{Q_a\,Q_b}{R^2}\,\hat{\mathbf{R}}_{ab} \tag{2}$$

[2]The value of G is $6.67{\cdot}10^{-11}$ $\mathrm{Nm^2/kg^2}$.

[3]Here light means all types of electromagnetic radiation, from radio waves to gamma rays. The light that our eyes are sensitive to is called the optical light, or the visible light.

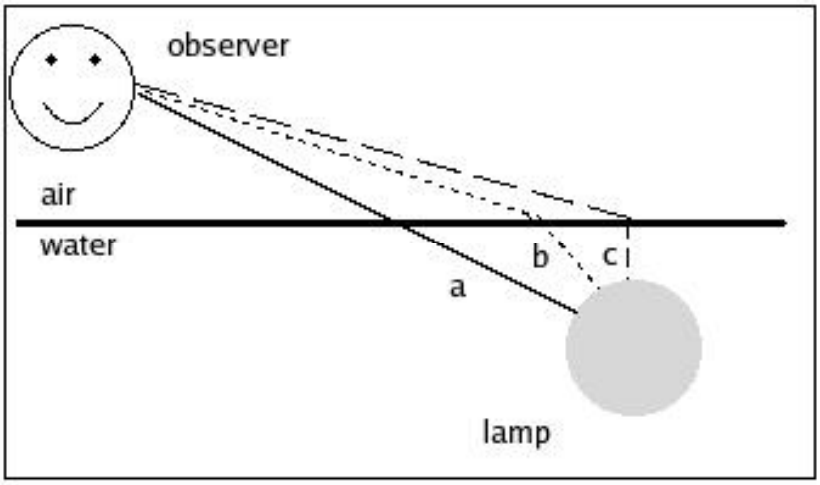

Figure 2: An observer exposed to light rays from a swimming-bath lamp.

where k_E is a constant, Q_a and Q_b are the charges of the objects, R is the distance and the vector $\hat{\mathbf{R}}_{ab}$ denotes the direction of the force. When using eq. (2) the force gets repulsive when the object exerting the force and the object experiencing the force has the same sign of charge, when the signs are different the force is attractive.

Equation (2) holds only if the charges are resting or moving with the same velocity relative each other, therefore it is called the electrostatic force. If one charge begin to accelerate or decelerate relative to the other, the electrostatic field will be disturbed. The disturbance will propagate outward from the accelerated charge with a constant velocity as a wave, an electromagnetic wave or *light*. In short, light is an electromagnetic wave that originates from a disturbance in the electromagnetic field, and what kind of light that is emitted depends on the velocity change of the charge, the faster accelerating, or decelerating, the shorter the wavelength of the emitted light.

1.3 Lensing of Light

Nothing travels faster than the speed of the light in vacuum and you need an infinite amount of energy to reach this velocity, so it is impossible, but it is possible to travel faster than light in other materials. Light goes slower in water than it does in air, something that can be seen in a swimming-bath with a lamp under the surface, see Fig. (2). Above the surface the lamp can be seen in one position, while under the surface the lamp is seen in another position. This is due to the fact that light always takes the path where the time function is stationary, i.e. at its minima, maxima and saddle points, this phenomena is called *Fermat's principle* after the French mathematician

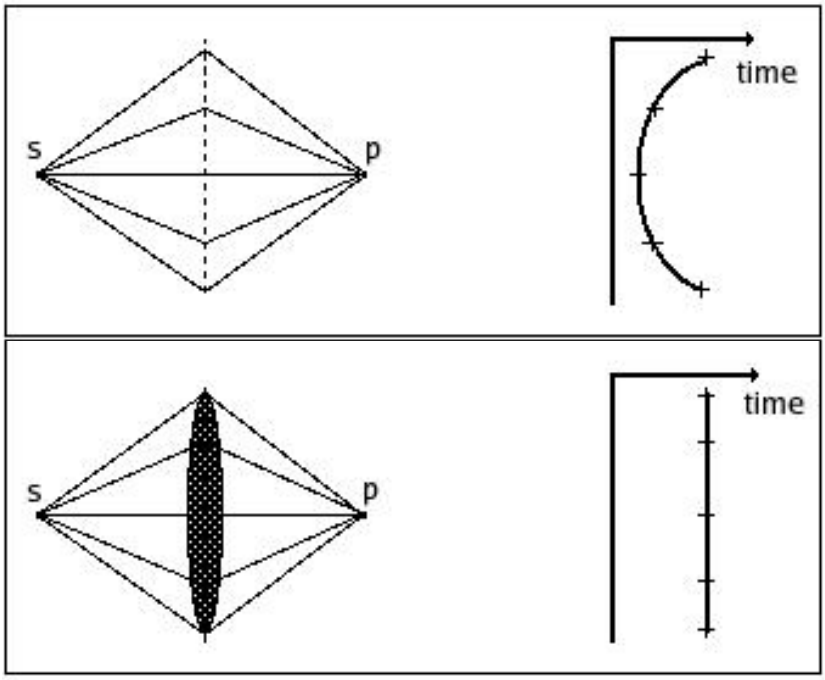

Figure 3: Time-analysis of some possible paths from a light source s to an observer at p. In the lower figure a trick on nature is played by a focusing lens (this figure is adapted from [6]).

Pierre de Fermat[4].

In Fig. (2) three different light paths are shown. Because light slows down in water, path a (solid) the shortest in distance is not the shortest in time. c (dashed) is the path that spends the longest time in air, but it turns out that path b (dotted) represents the path of the light. Thus, standing at the rim you will believe that the lamp is in path b's prolongation.

By constructing lenses some parts of a light beam can be slowed down. In Fig. (3), two different systems are shown where a point p receives light rays from a source s. According to Fermat's principle, in the upper figure p sees the light ray that has propagated straight from s, the plot to the right shows the differences in time arrival at p. In the lower figure a lens is inserted between the source and the observing point p. Since light goes slower through glass than air, the rays slows down a bit when they pass through the glass lens. By constructing the lens so the rays with the longest geometrical way spends the shortest time in glass, all rays will arrive at point p at the same time, shown in the right time-arrival plot. Therefore,

[4]Like many other physical phenomena, a light ray path is determined by probability. To say that light always travels the path where the time function is stationary is an approximation, but it will hold in this thesis.

the lens is focusing the rays and there will be a magnified image of s at p. The value of the magnification depends on the distances between the source, the lens and the observer.

This thesis is about gravitational lensing, i.e. a system where light rays are affected by the gravity from a massive object. So, in analogy with the lensing of light in Fig. (3) the massive object in Fig. (1) is lensing the light from the background source (assuming that the massive object is not transparent and blocking the straight rays).

2 Cosmology

2.1 About Cosmology

In cosmology the universe's origin, evolution and structure are studied. Today, the leading theory of the origin of the universe is the big bang theory, which states a very fast spatial expansion starting 13.6 billions years ago. Evidence have been found, and are still being found, that supports the theory of the big bang, e.g. the discovery of the expansion of the universe, the background radiation, the darkness of the sky (the fact that the starry sky is not filled with stars), the abundances of light elements like hydrogen and deuterium and the homogeneity of the universe (data showing that our location in the universe is not special) [20].

Modern observational cosmology began with the discovery of the expansion of the universe, made by Edwin Hubble 1929. Hubble found that distant galaxies, not members of the local group, are receding from us with a velocity proportional to their distance. According to the well known theory of gravity the expansion should decrease with time, but 1998 it was found that this expansion is accelerating [22], which makes up one of the deepest mysteries in cosmology: the force behind the accelerating expansion of the universe [20] [8].

On large scales, larger than 100 Mpc, the universe appears homogeneous and isotropic[5]. Homogeneous means that any measurable property of the universe is the same everywhere, the density has the same non-zero value everywhere at present time, and isotropic means that the universe looks the same in every direction. That the universe is homogeneous and isotropic constitutes the *cosmological principle*, introduced by Einstein 1917, before anything was known about the large-scale structure beyond our Galaxy. The cosmological principle is also taken to be valid at all epochs [20].

2.2 The Expansion

A light wave can be Doppler shifted in the same manner as a sound wave[6]. When observing a receding galaxy the emitted light becomes redder, i.e. the wavelength becomes longer, and if the galaxy is approaching the light becomes bluer. For a velocity v much smaller than the speed of the light c, the Doppler formula gives

$$\frac{\lambda_e - \lambda_o}{\lambda_e} = \frac{v}{c} \tag{3}$$

[5] 1 pc (parsec)= $3.085678 \cdot 10^{16}$m

[6] When a sound becomes Doppler shifted the tone gets higher when its approaching and lower when its receding.

where λ_o and λ_e are the observed and emitted wavelengths. The shift in the wavelength for all velocities is then defined by the *redshift*, z, as

$$z = \frac{\lambda_e - \lambda_o}{\lambda_e} \iff \frac{\lambda_o}{\lambda_e} = 1 + z. \tag{4}$$

According to the cosmological principle, the observed recession of galaxies follows the same pattern in whatever direction we look, and the universe remains homogeneous. Therefore, the overall effect of the expansion is a change of length scale. In cosmology the expansion of the universe is controlled by a single function of time, the *scale factor* function $R(t)$.

Assume that a distance AB has the length l_i at time t_i, then at time t its length is

$$l(t) = l_i \frac{R(t)}{R(t_i)}. \tag{5}$$

Differentiating eq. (5) with respect to time gives the relative velocity

$$v(t) = \frac{l_i}{R(t_i)} \frac{dR(t)}{dt} = \frac{\dot{R}(t)}{R(t)} l(t). \tag{6}$$

The velocity in eq. (6) is the expansion velocity of the distance between A and B, i.e. the points A and B are not moving but the space in every single point is expanding.

In cosmology the rate of expansion is characterized by the *Hubble parameter* H defined by

$$H = \frac{\dot{R}(t)}{R(t)}. \tag{7}$$

As one can see in eq. (7), the Hubble parameter is a function of time and independent of position, it is an observable measure of the rate at which the universe is expanding [20].

Equation (6) shows that, when observing a distant galaxy it is not the receding velocity that makes the light Doppler shifted, it is the expansion of the universe that is redshifting the light, i.e. the wavelength of the propagating photons expands. This gives the following relation between redshift and expansion

$$\frac{\lambda_0}{\lambda_e} = \frac{\nu_e}{\nu_0} = \frac{R(t_0)}{R(t_e)} = \frac{l_0}{l_e} = \frac{dt_0}{dt_e} = 1 + z \tag{8}$$

where ν is the frequency of the photon, the subscript 0 denotes the value at the present time. Here is also shown how a distant observer sees all physical processes slowed down with a factor $(1 + z)$, i.e. the observed time interval dt_0 is longer than the time interval dt_e measured at the location of the event.

2.3 Dark Energy

Throughout the 1920s it was taken for granted by cosmologists that the universe was static. In order to obtain a static distribution of matter 1917, Einstein added a constant in his field equations when he applied his theory of general relativity to the distribution of matter in the universe. Einstein called this constant the *cosmological constant*, denoted as Λ, which in the equations gave rise to an repulsion that could balance the gravity of the matter distribution.

In January 1930 at the Royal Astronomical Society in London, Eddington and de Sitter reached the conclusion that the static solution was not satisfactory and proposed a paradigm shift from a static to an expanding universe. However, a non-static solution was already found by Lemaître and later it was discovered that Friedmann also had found a solution 1922. Finally, Robertson and Walker independently showed that there are no alternative solutions to the field equations. As a result, the solution of Einstein's theory for an expanding universe is called the Friedmann, Lemaître, Robertson-Walker model, abbreviated as FLRW [20].

The unknown repulsive force behind the accelerating expansion is often attributed to different forms of *dark energy*. Two facts we know about dark energy are that it has negative pressure and that it makes up about 70 % of the universe.

Different kinds of mechanisms driving the accelerating expansion would produce different observable consequences. Today, the simplest interpretation of the accelerating universe is in terms of the cosmological constant or the *vacuum energy*. According to quantum theory vacuum is not empty, subatomic particles and their antiparticles creates and annihilates in vacuum, the *Casimir effect*. However, calculations shows that the vacuum density is 10^{122} times as big as the observed dark energy [2], and such a value would cause the acceleration to rip apart galaxies, stars, atoms and life would be impossible. Since we cannot ignore quantum mechanics something must decrease this vacuum energy [19].

Several teams of researchers are conducting and planning experiments to investigate this unknown force. On the cosmic scale, astronomers are developing new sky surveys searching for supernovae and using the effects from gravitational lensing to determine the cosmological parameters. On a small scale, particle physicists are doing experiments that may reveal whether the answer to the mysteries lies in hidden spatial dimensions or in undiscovered fundamental particles.

2.4 Geometries

If the Pythagorean law holds between the points (x, y) and $(x + \delta x, y + \delta y)$, the geometrical properties are Euclidean and, when we consider the limit as

the separation of the two points goes to zero, the infinitesimal distance ds between the points is given by

$$ds^2 = dx^2 + dy^2. \tag{9}$$

When space is curved like on the surface of a sphere, the geometry is non-Euclidean and the Pythagorean law will not hold, instead the distance law is given by

$$ds^2 = r^2 + d\theta^2 + r^2 \sin^2\theta \, d\phi^2 \tag{10}$$

where r is the radius and θ and ϕ are the two spherical angles. For instance, on a spherical surface the angles on a triangle will exceed $180\,^\circ$ and if the surface is saddle shaped the sum is less than $180\,^\circ$ [20].

Now, if we turn to special relativity we define a four-dimensional geometry called *spacetime*, based on our three spatial dimensions and the dimension of time[7]. Clocks run differently in different frames depending on their velocities, and the time in a given frame is called *proper time*, τ. Proper time is invariant when one changes frame, since it is a property for a given particle and not the coordinate system. In analogy with the Pythagorean law, the geometry in special relativity defines a distance in spacetime as

$$ds^2 = c^2 \, d\tau^2 = c^2 \, dt^2 - dx^2 \tag{11}$$

where c is the speed of the light, t is time and x is the distance in space simplified to one dimension instead of three [20].

General relativity is all about proper time and gravity, special relativity is just a local part of general relativity. General relativity gives an expression for the proper time in a global frame. The basic idea is that the spacetime in general relativity is allowed to have a more general geometry, e.g it can be curved and expanding. The geometry, or the metric, that Friedmann, Lemaître, Robertson and Walker found when solving Einstein's field equations for a dynamic universe defines a distance in spacetime as

$$ds^2 = c^2 \, dt^2 - R(t)^2 \left(\frac{dr^2}{1 - kr^2} + r^2 \, d\theta^2 + r^2 \sin^2\theta \, d\phi^2 \right). \tag{12}$$

This equation is usually abbreviated as the FLRW-metric [20].

In eq. (12) the curvature factor k shows up. This factor can have three different values depending on the curvature of the universe. In a $k = 1$ universe, the spacetime is positively curved and the universe is finite or closed. In a crude analogy to a three-dimensional geometry we can think of it as the surface on a sphere. In a $k = -1$ universe, the spacetime is negatively curved and the universe is infinite or open, in three dimensions we can crudely think of it as a surface on saddle. Finally, in a $k = 0$ universe, the spacetime is flat and the universe is infinite [20].

[7] In fact time is distance, you can measure a distance in seconds as well as in meters.

2.5 Densities

The foundation stone of the standard model of cosmology is the FLRW-metric, and what then determines the dynamics of the universe are the *energy density parameters.*

Consider macroscopically the universe at all times as a gas of particles with a density ρ. These particles can now be representing galaxies or clusters of galaxies as well as photons. Einstein's field equations then yield one of the most fundamental equations of cosmology the *Friedmann equation*, which tells us how the scale factor changes with time

$$\left(\frac{dR}{dt}\right)^2 = \frac{8}{3}\pi G\rho R^2 - kc^2 + \frac{1}{3}\Lambda R^2. \tag{13}$$

The mean density $\rho(t)$ includes densities from all kinds of matter (both visible and dark matter[8]) and radiation and can therefore be written as $\rho = \rho_m + \rho_r$. The cosmological constant is given by $\Lambda = 8\pi G\,\rho_\Lambda$. Using these expressions in combination with eq. (7) we can rewrite the Friedmann equation as

$$-kc^2 = R^2 H^2\left[1 - \frac{8\pi G}{3H^2}\left(\rho_m + \rho_r + \rho_\Lambda\right)\right]. \tag{14}$$

This equation shows how the curvature of the universe is related to the density in the universe. As discussed above, k can have three different values which now relates to eq. (14) as

$$k = 0 \implies \quad \rho_m + \rho_r + \rho_\Lambda = \frac{3H^2}{8\pi G}, \tag{15}$$

$$k = -1 \implies \quad \rho_m + \rho_r + \rho_\Lambda < \frac{3H^2}{8\pi G}, \tag{16}$$

$$k = +1 \implies \quad \rho_m + \rho_r + \rho_\Lambda > \frac{3H^2}{8\pi G}. \tag{17}$$

These relations show that the curvature of the universe is determined by the right hand term in eqs. (15)- (17), the *critical density* defined as

$$\rho_c = \frac{3H^2}{8\pi G}. \tag{18}$$

The densities from matter, radiation and the cosmological constant can then be expressed in terms of the critical density as

$$\Omega_i = \rho_i/\rho_c \tag{19}$$

[8]Dark matter means all kinds of matter that we can not see, e.g. planets, brown dwarfs, neutrinos, black holes etc.

which gives

$$\Omega_M = \frac{8\pi\, G\, \rho_M}{3\, H_0^2}, \tag{20}$$

$$\Omega_R = \frac{8\pi\, G\, \rho_R}{3\, H_0^2}, \tag{21}$$

$$\Omega_\Lambda = \frac{\Lambda}{3\, H_0^2}, \tag{22}$$

where the uppercase letters denote the values at the present time [20].

By defining the curvature energy density parameter as

$$\Omega_K = -\frac{kc^2}{R(t_0)^2\, H_0^2}, \tag{23}$$

we can rewrite the Friedmann equation as

$$1 = \Omega_M + \Omega_R + \Omega_\Lambda + \Omega_K. \tag{24}$$

Since the present value of $\Omega_K \approx 0$ and the present value of Ω_R is so small that it can be neglected, the destiny of the universe is determined by the balance between Ω_M and Ω_Λ [20] [8]. Equation (24) can then be rewritten as

$$\Omega_\Lambda = 1 - \Omega_M. \tag{25}$$

2.6 Distances

Our view of very distant objects is complicated by the cosmic expansion that increases the wavelength of light and by the curved spacetime that it passes through. When we view a galaxy its brightness is diminished by one power of $(1 + z)$ because every received photon carries less energy, and another power because they arrive at a slower rate, see eq. (8) [27].

When we receive the light from a galaxy emitted at time t_1, the light is spread out over a sphere with the area $4\pi r^2(t_1)R^2(t_0)$, where $r(t_1)$ is the galaxy's radial coordinate [27]. Therefore, the flux S of energy that we receive is related to the total or bolometric luminosity L by

$$S = \frac{L}{4\pi\, r^2(t_1)\, R^2(t_0)\, (1+z)^2} \equiv \frac{L}{4\pi\, d_L^2(z)} \tag{26}$$

where d_L is the *luminosity distance*. Thus, the luminosity distance to an event at position r_1 and time t_1 is given by

$$d_L = R(t_0)\, (1+z)\, r_1. \tag{27}$$

Another important cosmological distance is the *angular distance* d_A, which tells us how large an object will appear when it is seen at redshift z.

If a galaxy at a distance d subtends an angle α on the sky, the size of the galaxy D is given by the *small angular formula*

$$D = \alpha\, d. \tag{28}$$

However, we observe the size D when the light was emitted, therefore d must be equal to the galaxy's radial coordinate multiplied with the scale factor at the time of emission [27]. This gives the angular distance to an event at position r_1 and time t_1 as

$$d_A = R(t_1)\, r_1. \tag{29}$$

Combining eqs. (8), (27) and (29) gives the radial coordinate as

$$r_1 = \frac{d_A\,(1+z)}{R(t_0)}. \tag{30}$$

Consider now a radially incoming light ray to an observer, situated at the origin of a r, θ, ϕ coordinate system so θ and ϕ are both constant, and $d\theta = d\phi = 0$. Inserting these values in eq. (12), together with the condition that light rays move of paths of zero proper time gives

$$\frac{dr}{dt} = \frac{\sqrt{1-kr^2}}{R(t)}\, c. \tag{31}$$

Multiplying eq. (31) with $R(t_0)$ and using eq. (8) gives

$$R(t_0)\frac{dr}{\sqrt{1-kr^2}} = c\,(1+z)\,dt. \tag{32}$$

In [2] this useful differential equation is given

$$\frac{dt}{dz} = \frac{1}{H_0\,(1+z)\,[(1+z)^2\,(1+\Omega_M\,z) - z\,(2+z)\,\Omega_\Lambda\,]^{1/2}}. \tag{33}$$

Equation (32) together with eq. (33) gives

$$R(t_0)\int_0^{r_1}\frac{dr}{\sqrt{1-kr^2}} = c\int_0^{z_1}\frac{dz}{H_0\,[(1+z)^2(1+\Omega_M z) - z(2+z)\Omega_\Lambda]^{1/2}}. \tag{34}$$

After some calculations, with the use of eqs. (25) and (30), eq. (34) gives the angular distance for a flat universe ($k = 0$) as

$$d_A(H_0,\,\Omega_M,\,z) = \frac{c}{H_0\,(1+z)}\int_{z_0}^{z_1}\frac{d\acute{z}}{[\Omega_M(\,(1+\acute{z})^3 - 1) + 1]^{1/2}}. \tag{35}$$

In the next chapter we show how the time delays in a gravitational lensing system depend on the angular distances, which through eq. (35) are sensitive to the cosmology.

3 Gravitational Lensing

3.1 A Short History of Gravitational Lensing

Although gravitational lensing (see Fig. (1)) in a cosmological context was discovered 1979, the possibility of its existence had been suspected long before. Albert Einstein [5] proposed that rays of light could be bent by a gravitational field with celestial objects acting like lenses and form magnified images. At the same time he thought that the angular image splitting from stellar-mass lenses was too small to be resolved by an optical telescope. This was an outgrowth of his theory of general relativity, where the presence of matter can curve spacetime, and the path of a light ray will be deflected as a result. Einstein predicted a shift in a star's apparent position by 1.74 arcseconds when it is lensed by the sun. During a total solar eclipse 1919 at the island of Principe, the British astronomer Arthur Eddington took photographs of the sky around the sun and found out that nearby stars had moved just the angle predicted by Einstein [18].

1962 at Oslo University, Sjur Refsdal was defending his diploma-thesis and got rejected on his gravitational lensing part, the examiner claimed one had to use physical optics instead of geometrical optics which Refsdal had done. Anyway, he did not give up proving that geometrical optics was right, and that was the way he came to calculate time delays [12], i.e. the difference in travel time for light compared with the travel time without any intervening lens. In 1964, Refsdal [21] then described how the Hubble constant could in principle be measured by gravitational lensing of a variable source [18].

With the discovery of quasars 1963 [23], which is a good class of sources for studying the effects of gravitational lensing, the thought of observing gravitational lensing were brought up to daylight again. Quasars are active galactic nuclei so bright that they outshine their host galaxies. They are very distant objects so the probability is relatively high that something massive is intervening between them and us. They are much smaller than typical scales of galaxy lenses and their optical region is very compact, the resulting magnification can therefore be large and multiple images can be separated and detected [18].

What had been a dream for a few theoreticians became reality 1979 when Walsh, Carswell, Weymann [30] discovered the first example of gravitational lensing in a cosmological context, the quasar QSO 0957+561A,B. The determination of the Hubble parameter by using the time delay effect from gravitational lensing system now became a realistic possibility. Gravitational lensing has nowadays developed into a powerful tool to study important questions in astrophysics and cosmology [18].

Today, sky surveys have found a lot of gravitational lensed objects, one year ago (June 2003) 72 multiple image systems were known [24] and the

list continues to grow with improved observing techniques. In 1986 the first Einstein ring was discovered; the radio source JVAS B1938+666, lensed like a ring by an intervening galaxy. Also discovered in 1986 was a new lensing phenomena; strongly giant arcs around clusters of galaxies, and after measuring the redshifts of one of the arcs one could determine that it was an image of a background galaxy [24].

Even better time delays than from quasars could be provided from supernovae [11], but no lensed supernova has been found yet. A supernova occurs when a star between 10-40 solar masses stops burning and shrinks due to its on gravity. The star will then keep shrinking until the core gets degenerated with neutrons, the degenerated core can then not shrink anymore and the sudden stop of the collapse will produces an outgoing shock wave, an explosion, i.e. a supernova of Type II [27].

Another type of supernova occurs when the remainder of a star that was less massive than 10 solar masses during its main sequence[9], i.e. a white dwarf, accretes mass from its binary companion. This mass accretion makes the white dwarf exceed the Chandrasekhar limit, where the star can not support its on weight, and will then explode in supernova of Type Ia [27].

Supernovae of Type Ia are currently considered as the best astrophysical sources with known luminosity, i.e. standard candles [8]. They have three important features required of a standard candle; they are very luminous, the dispersion of their absolute magnitude about the mean is small and finally, the physical characteristics of low and high redshifts are very similar [20].

3.2 Basics of Gravitational Lensing

In general, light propagation in a curved spacetime is a complicated problem. However, for almost all cases of relevance to gravitational lensing, we can assume that the geometry is described by the FLRW-metric (see section 2.4) and that the matter responsible for the lensing are no more than local perturbations in an otherwise homogeneous universe [18].

When light paths propagates from a source past a lens to an observer (see Fig. (1)) the paths can be broken up in three zones. In the first zone, light goes from the source to a point close to the lens through a unperturbed spacetime. In the second zone, the vicinity near the lens, the light is deflected. When studying the deflection inside the second zone we can assume a local flat spacetime which is weakly perturbed by the Newtonian gravitational potential, arisen from the lens's mass distribution. Our assumptions holds if the Newtonian potential Φ is small, $\mid \Phi \mid \ll c^2$, and if the velocity v of the lens is small, $v \ll c$. Finally, in the third zone light goes through an unperturbed spacetime from the lens toward the observer [18].

[9]The main sequence is a star's epoch of hydrogen burning.

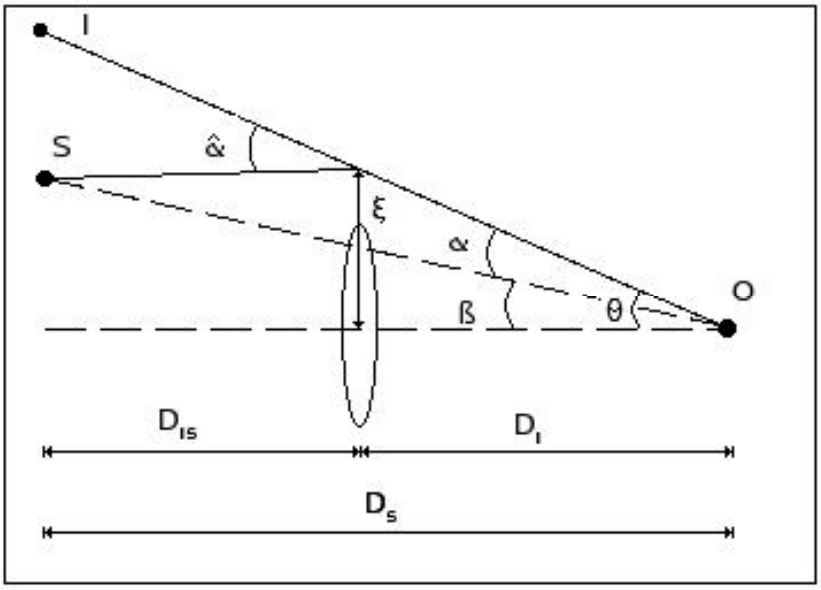

Figure 4: Sketch of typical gravitational lens system. A light ray propagates from a source S to an observer O, passing a lens at distance ξ, i.e. the impact parameter. The angular separations of the source and the image seen from the observer, are β and θ respectively. $\hat{\alpha}$ is the deflection angle and α is the reduced deflection angle. The distance between the observer and the lens is D_l, between the observer and the source, D_s and between the lens and the source, D_{ls}.

3.2.1 The Lens Equation

In Fig. (4) a typical gravitational lens system is shown with an optical axis defined as a straight line through the lens center and the observer. A light ray is deflected by the angle $\hat{\alpha}$ when propagating from a source S to an observer O, β is the angle between the optical axis and the true position and θ is the angle between the optical axis and the image position I. ξ is the transverse distance between the optical axis and the point where the ray pass the lens. The angular distances are; D_l between observer and lens, D_s between observer and source and D_{ls} between source and lens.

Assuming that the angles are very small and approximating, e.g. $\tan\beta \approx \beta$, one finds that

$$\beta = \theta - \frac{D_{ls}}{D_s}\,\hat{\alpha}. \tag{36}$$

In gravitational lensing it is convenient to introduce the reduced deflection angle α [18] [24], which is the angle that separates the true position and the image (of course one can not see this angle). From the geometry in

Fig. (4) one can show that the reduced deflection angle is

$$\alpha = \frac{D_{ls}}{D_s}\,\hat{\alpha}. \tag{37}$$

Combining eqs. (36) and (37) gives

$$\beta = \theta - \alpha(\theta). \tag{38}$$

This is the *lens equation* relating a source's true position to the observed. In general, the equation is nonlinear which makes multiple images possible [24].

3.2.2 Deflection Angles

The effects from the spacetime curvature on light paths can be expressed in terms of a refractive index n, which is given by [18]

$$n = 1 - \frac{2}{c^2}\,\Phi = 1 + \frac{2}{c^2}\,|\Phi|. \tag{39}$$

The deflection angle of a light ray when passing through a gravitational field is given by (e.g. [18])

$$\hat{\alpha} = -\int \nabla_\perp\, n\, dl = \frac{2}{c^2}\int \nabla_\perp\, \Phi\, dl. \tag{40}$$

This equation shows that the deflection angle is the integral of the perpendicular gradient of n along the light path. In all cases of interest this deflection angle becomes very small, and we can therefore simplify our calculations by integrating $\nabla_\perp\, n$ along an unperturbed light ray, instead of along the deflected ray [18].

Consider the point mass lens in Fig. (5), the Newtonian gravitational potential around the point mass is given by

$$\Phi(b,\, z) = -\frac{G\,M}{\sqrt{b^2 + z^2}} \tag{41}$$

where b is the distance between the point mass and the unperturbed light ray and z is the distance along the unperturbed light ray where the deflection occurs. By using eq. (40), a point mass lens gives the deflection angle

$$\hat{\alpha} = \frac{2}{c^2}\int_{-\infty}^{\infty} \nabla_\perp\, \Phi\, dz = \frac{4\,G\,M}{c^2\,b}. \tag{42}$$

Equations (41) and (42) shows that most of the deflection occurs within $\Delta z \sim \pm b$ to the point of closest encounter between the ray and the point mass. This Δz is very small compared with the distances between source and lens and lens and observer, the lens can therefore be considered as very

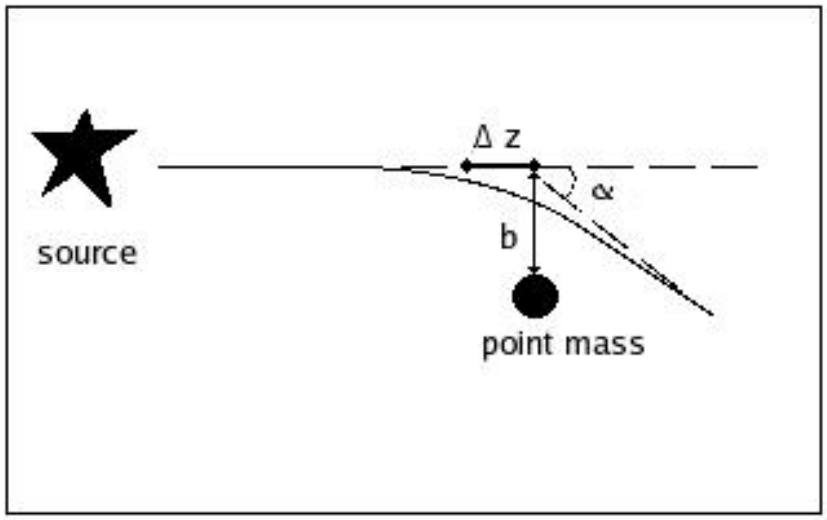

Figure 5: Light deflection by a point mass lens. Most of the deflection occurs within $\Delta z \sim \pm b$ (this figure is adapted from [18]).

thin and the mass distribution of the lens can be projected along the line-of-sight, like a mass sheet perpendicular to the line-of-sight. The plane of this mass sheet is called the *lens plane*. The deflection angle depends solely on the mass sheet [18] [24], which is characterized by its surface mass density

$$\Sigma(\xi) = \int \rho(\xi,\, z)\, dz \tag{43}$$

where the impact parameter ξ is a two-dimensional vector in the lens plane. The deflection angle at ξ is the sum of the deflection contributions from all the mass element in the lens plane [18] [24], i.e.

$$\hat{\alpha}(\xi) = \frac{4\,G}{c^2} \int \frac{(\xi - \acute{\xi})\, \Sigma(\acute{\xi})}{\mid \xi - \acute{\xi} \mid^2}\, d^2\acute{\xi}. \tag{44}$$

In the case of a circularly symmetric lens, we can shift the coordinate system to the center of symmetry and reduce the deflection to a one-dimensional problem [18]. The deflection angle directed toward the optical axis is then given by

$$\hat{\alpha}(\xi) = \frac{4\,G\,M(\xi)}{c^2\,\xi} \tag{45}$$

where ξ is the distance from the lens center and $M(\xi)$ is the mass enclosed within radius ξ given by

$$M(\xi) = 2\pi \int_0^{\xi} \Sigma(\acute{\xi})\, \acute{\xi}\, d\acute{\xi}. \tag{46}$$

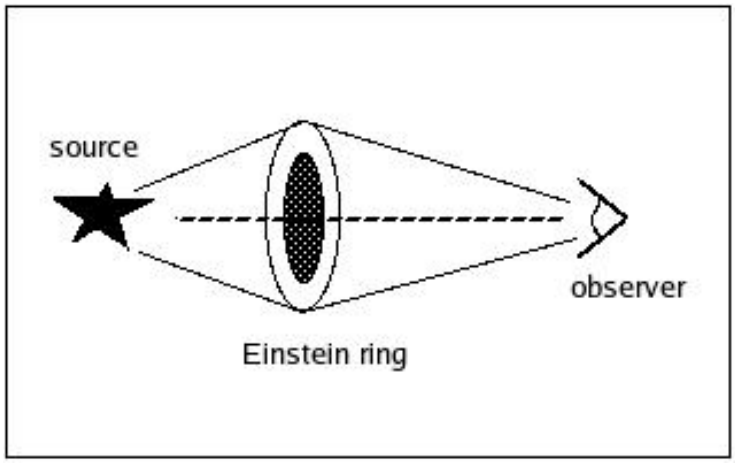

Figure 6: When the lens and observer are perfectly aligned the image becomes a ring, i.e. Einstein ring.

3.2.3 Einstein Radius

If a source lies exactly on the optical axis ($\beta = 0$) and is lensed by a circular symmetric lens, a ringlike image can occur; an *Einstein ring* (see Fig. 6). The Einstein radius is important in gravitational lensing. For instance, when a source is multiple imaged the angular separations between the images is of order two Einstein radii, and in many models the projected Einstein ring on the source plane roughly represents the source's border area between getting multiple imaged or not [18].

The Einstein radius can be found by consider a circularly symmetric lens with an arbitrary mass profile. According to eqs. (45), (37) and (38), the lens equation gives

$$\beta = \theta - \frac{D_{ls}}{D_l D_s} \frac{4G\,M(\theta)}{c^2\,\theta}. \tag{47}$$

By setting $\beta = 0$ in eq. (47) one obtains the *Einstein radius* as

$$\theta_E = \left[\frac{4\,G\,M(\theta_E)}{c^2} \frac{D_{ls}}{D_l D_s} \right]^{\frac{1}{2}}. \tag{48}$$

3.2.4 Magnification

Since gravitational light deflection is not associated with emission or absorption of light, the surface brightness is preserved and the intensity of the images can be magnified. The total flux received from a gravitationally lensed object is proportional to the ratio between the solid angles of the image and the source. The magnification factor is denoted μ and is, for a

circular symmetric lens, given by

$$\text{magnification} = \frac{\text{image area}}{\text{source area}} = \frac{\theta}{\beta}\frac{d\theta}{d\beta} = \mu. \tag{49}$$

3.2.5 The Time Delay Function

Consider again the light ray in Fig. (4) which propagates from a source to a point on the lens plane, and then from there to an observer. For a given path there is a geometrical and a gravitational time delay, i.e. the light ray is delayed relative to propagation in vacuum [3].

The geometrical contribution is the extra light path that arises when the lens deflects the light ray. In appendix A it is shown that the geometrical time delay can be written as

$$\Delta t_{geo} = \frac{1}{2}\left[\frac{1+z_l}{c}\right]\left[\frac{D_l D_s}{D_{ls}}\right](\theta-\beta)^2. \tag{50}$$

The gravitational time delay arises in the vicinity of the lens where, as in optics, the refractive index n slows down the speed of the light to c/n. The gravitational time delay Δt_{gr} is obtained by integrating over the light path from the observer to the source

$$\Delta t_{gr} = -(1+z_l)\int \frac{2}{c^3}\,\Phi\, dl. \tag{51}$$

where the redshift factor appears due to eq. (8).

Writing

$$\Delta t_{gr} = -\left[\frac{1+z_l}{c}\right]\left[\frac{D_l D_s}{D_{ls}}\right]\psi(\theta) \tag{52}$$

where $\psi(\theta)$ is the *deflection potential* [24], defined in [18] as a the projection of the Newtonian potential along the line-of-sight as (see eq. (41))

$$\psi(\theta) = \frac{D_{ls}}{D_l\, D_s}\frac{2}{c^2}\int \Phi(D_l\,\theta,\, l)\, dl, \tag{53}$$

the total time delay then takes the form

$$\Delta t_{tot} = \Delta t_{geo} + \Delta t_{gr} = \left[\frac{1+z_l}{c}\right]\left[\frac{D_l D_s}{D_{ls}}\right]\left[\frac{1}{2}(\theta-\beta)^2 - \psi(\theta)\right]. \tag{54}$$

According to Fermat's principle $\nabla_\theta\, \Delta t_{tot}(\theta) = 0$, so the lens equation (eq. (38)) can be rewritten as a gradient

$$\nabla_\theta\left[\frac{1}{2}(\theta-\beta)^2 - \psi\right] = 0 \tag{55}$$

where the gradient of ψ with respect to θ gives the reduced deflection angle as (cf. eq. (42))

$$\nabla_\theta\,\psi = D_l\,\nabla_\xi\,\psi = \frac{2}{c^2}\frac{D_{ls}}{D_s}\int \nabla_\perp\,\Phi(D_l\,\theta,\, z)\, dz = \alpha. \tag{56}$$

This means that the competition between the geometric and the gravitational delays leads to the formations of images at the functions stationary points (minima, maxima and saddle points), so for a given source position β one can find all the associated positions θ [18] [14].

Interpreting time delays requires a model for the lens's gravitational potential, and in most cases the uncertainties in this model will then dominate the uncertainties in the calculated cosmological parameters that the time delay function can provide. Therefore, due to the gravitational delay, time delay lenses provides a probe of the dark matter distribution in the lens, since they measure the matter distribution in the lens [14].

3.3 Types of Gravitational Lensing

Depending on the mass distribution, the shape of the lens and the impact parameter, there are different types of gravitational lensing, including; strong-, weak- and microlensing. Below is a short description of the these types [27] [2].

3.3.1 Strong Lensing

Strong lensing is the most extreme bending of light, causing more than one image to appear, so called multiple images. If the source is time varying, the multiple images will vary with time as well, which makes it possible to measure time delay differences between the images. If the lens is circularly symmetric and lies perfectly aligned with the source, a ring-image will appear; a so called *Einstein ring* (see Fig. 6). More often the shapes of the images are stretched out and curved as arcs [27].

3.3.2 Weak Lensing

Weak lensing appears when the lens is not strong enough to make multiple images, instead one single image will appear. The source can still be distorted, both magnified and stretched out as an arc. If all sources were well known, weak lensing could then be used to get informations about the lens. Weak lensing is a useful tool to measure the distribution of mass, since it measures all kind of masses both the luminous matter and the dark matter [27].

3.3.3 Microlensing

Microlensing occurs when the lensing effect affects the luminosity of one source, a faint source can thereby get visible for our detectors, e.g. when a massive object passes in front of a source and multiple images can not be resolved. This technique is used to map the Galactic density of dark matter

objects such as MACHOs (Massive Astrophysical Compact Halo Objects), e.g. brown dwarfs, neutron stars, black holes and planets [2].

3.4 The Singular Isothermal Sphere Model

A simple but realistic starting point for modeling lens potentials is the *Singular Isothermal Sphere Model*, abbreviated as the SIS-model [14]. In this model a galaxy's stars and other mass components are macroscopically considered as an ideal gas of particles with density ρ and mass m. The equation of state for an ideal gas then takes the form

$$p = \frac{\rho\, k\, T}{m} \tag{57}$$

where k is the Boltzmann constant[10]. In thermal equilibrium, the temperature T is related to the velocity dispersion σ_v of the stars through

$$m\sigma_v^2 = k\, T. \tag{58}$$

Usually one assumes that a stellar gas is isothermal, which gives that σ_v is constant across the galaxy. Narayan and Bartelmann (1995) [18] gives a solution of eq. (57) as

$$\rho(r) = \frac{\sigma_v^2}{2\pi\, G}\frac{1}{r^2} \tag{59}$$

where r is the radius of the sphere.

3.4.1 SIS- Deflection Angle

Projecting the mass distribution from eq. (59) along the line-of-sight, the surface-mass density is obtained after using eq. (59) in eq. (43) as (see appendix B)

$$\Sigma(\xi) = \frac{\sigma_v^2}{2\, G}\frac{1}{\xi}. \tag{60}$$

By combining eqs. (45), (46) and (60), the deflection angle for a SIS-distribution takes the form

$$\hat{\alpha} = 4\pi\, \frac{\sigma_v^2}{c^2}. \tag{61}$$

The Einstein radius for a SIS is then given by eq. (38) as

$$\theta_E = \hat{\alpha}\, \frac{D_{ls}}{D_s} = \alpha. \tag{62}$$

Although the lens equation for a SIS is essentially one-dimensional, multiple images do appear. To clarify, consider a source located at a positive coordinate from the optical axis of a SIS-lens, i.e. β has a positive value.

[10]The value of the Boltzmann constant is $k = 1.380658 \cdot 10^{-23}$ J/K

Because the image position θ is always directed toward the optical axis, the solutions of the lens equation are

$$\theta_{\pm} = \beta \pm \theta_E. \tag{63}$$

However,

$$\beta > \theta_E \implies \theta_- = \beta - \theta_E < \beta$$

which is impossible (see Fig. 4). Therefore, eq. (63) holds only if the conditions $\beta < \theta_E$ is satisfied.

3.4.2 SIS- Time Delay Function

Consider a SIS-lens producing two images a_1 and a_2 at the angles θ_{a_1} respective θ_{a_2} from the optical axis. Combining eqs. (56) and (61) gives the deflection potential for an SIS-lens as

$$\nabla_{\theta_i}\psi = 4\pi \frac{D_{la}}{D_a}\frac{\sigma_v^2}{c^2} = \alpha \quad \implies \quad \psi(\theta_i) = \alpha\theta_i. \tag{64}$$

Using this lens potential expression in eq. (54), the time delay between the two images a_1 and a_2 can be calculated as (see appendix C)

$$\Delta t_{sis} = \Delta t_{a_2} - \Delta t_{a_1} = \frac{1}{2}\left[\frac{1+z_l}{c}\right]\left[\frac{D_l D_a}{D_{la}}\right](\theta_{a_1}^2 - \theta_{a_2}^2). \tag{65}$$

Thus, the SIS-model suggests that the determination of the cosmological parameters[11] is reduced to a problem of measuring the time delays, the redshifts and the positions of the images [14].

3.5 Power Law Lens Potential Model

Numerical simulations of Cold Dark Matter models show that dark matter halos exhibit a universal density profile with a central slope $\rho \propto r^{-\eta}$, with $\eta \approx 1 - 1.5$, and at large radii the profile steepens to $\rho \propto r^{-3}$ [17].

A general expression for a gravitational lens potential is given as [14]

$$\psi(\theta_i) = \frac{\theta_E^2}{(3-\eta)}\left(\frac{\theta_i}{\theta_E}\right)^{3-\eta} \tag{66}$$

where η is the *logarithmic slope of the density parameter* [13]. This potential model is called the *power law lens potential*. For $\eta = 2$, this model corresponds to a SIS-potential and for the limit $\eta \to 3$ it approaches a point mass potential [14].

[11] The cosmological parameters H_0 and Ω_M appears in the angular distance expressions.

3.5.1 Power Law Lens Potential- Time Delay Function

When a gravitational lensing system produces two images, a_1 and a_2, one can define an annulus of average angle

$$\langle\zeta\rangle = \frac{\theta_{a_1} + \theta_{a_2}}{2} \tag{67}$$

and width

$$\Delta\zeta = \theta_{a_1} - \theta_{a_2}. \tag{68}$$

By expanding the expression for the power law lens time delay in [13] as a series in the ratio $\Delta\zeta/\langle\zeta\rangle$, the time delay can be approximated as

$$\Delta t(\eta) = \frac{1}{2}\left[\frac{1+z_l}{c}\right]\left[\frac{D_l D_a}{D_{la}}\right](\theta_{a_1}^2 - \theta_{a_2}^2)\,(\eta-1)\left[1 - \frac{(2-\eta)^2}{12}\left(\frac{\Delta\zeta}{\langle\zeta\rangle}\right)^2 + \mathcal{O}\left(\frac{\Delta\zeta}{\langle\zeta\rangle}\right)^3\right]. \tag{69}$$

Assuming that $\Delta\zeta/\langle\zeta\rangle$ is small, higher-order terms can be ignored and eq. (69) can be rewritten as

$$\Delta t(\eta) \approx \frac{1}{2}\left[\frac{1+z_l}{c}\right]\left[\frac{D_l D_a}{D_{la}}\right](\theta_{a_1}^2 - \theta_{a_2}^2)\,(\eta-1)\left[1 - \frac{(2-\eta)^2}{3}\left(1 - \frac{2\theta_{a_2}}{\theta_{a_1}+\theta_{a_2}}\right)^2\right]. \tag{70}$$

Compared with the time delay difference for a SIS-model this model also requires a value for the logarithmic slope of the density parameter.

Since the expressions for the angular distances includes H_0 and Ω_M, the value of η, H_0, and Ω_M can be estimated with eq. (70) by using time delays from multiple images. By finding two or more objects multiple lensed by the same lens, their time delay differences can for instance be divided with each other and thereby reduce some factors in eq. (70), and probably make better parameter estimations.

4 Double Objects Lensing

Hubble Space Telescope (HST) observations have found families of multiple images with different measured spectroscopic redshifts [10], but these observations are lensed galaxies so they are bad candidates for measuring time delays. In the cluster Abell 2218, Soucail, Kneib and Golse (2004) [26] have studied 4 multiple images to determine the cosmological parameters Ω_M, Ω_Λ and w (the equation of state parameter). The basic idea in their method is that each family of multiple images constrains the cluster potential, and as this lensing test depends on the angular distances D_{ls}/D_s it also depends on the cosmological parameters, eq. (35). Their method is an extended version of Link and Pierce (1998) [15] work on determination of cosmological parameters using gravitational lensing system.

Sharon, *et al* (2004) [25] has found over 130 images of 35 lensed galaxy families behind the lensing cluster A1689. They calculated the surface mass distribution in A1689 and found it to flatten steadily toward the center. They have also found the mass to light ratio 30 % larger than any other well-studied cluster. Due to the redshift of the lens, $z = 0.18$, the dependence on cosmological parameters is weak and they could not constrain the cosmological parameters with accuracy [25].

No one has yet found a system with two quasars or supernova multiple lensed by the same lens, a so called DOL-system with measurable time delays. If such a DOL-system was found one could use eq. (70) to determine some cosmological parameters and the matter distributions of the lens.

4.1 About Double Objects Lensing Simulations

Different DOL-system can be simulated by changing the measurable parameters, i.e. σ_v, z_i and θ_i, from now on called the *observables*. In my simulations I consider the time delay one gets from a power law lens, eq. (70), as the *theoretical time delay*, Δt_{th}, and the *observed time delay*, Δt_{obs}, as the value one gets from a SIS-lens. Therefore, my simulated observed time delays are calculated by combining eqs. (35), (65) and (76) with the values for H_0 and Ω_M as [29]

$$\begin{cases} H_0 &= 70 \quad [\text{km s}^{-1}\ \text{Mpc}^{-1}] \\ \Omega_M &= 0.30 \end{cases} \tag{71}$$

The true values for the varying parameters, i.e. H_0, Ω_M and η, are then estimated with a χ^2-test, with the theoretical time delays against the observed time delay.

4.1.1 χ^2-test

A χ^2-test is a statistical tool for investigating whether an observed distribution is consistent with an expected theoretical distribution [28]. The χ^2 is

simply a sum of squares with the general form

$$\chi^2 = \sum_1^n \left(\frac{\text{theoretical value} - \text{observed value}}{\text{standard deviation}} \right)^2 \tag{72}$$

where n is the number of measurements. The agreement is best where $\chi^2 = \chi^2_{min}$, i.e. where the theoretical value approaches the observed.

When χ^2-testing time delays the χ^2 takes the form

$$\chi^2 = \sum \frac{(\Delta t_{th}(\eta, \Omega_M, H_0) - \Delta t_{obs})^2}{\sigma^2_{th} + \sigma^2_{obs}} \tag{73}$$

where σ_{th} is the uncertainty in the power law time delay and σ_{obs} is the uncertainty in the observed time delay.

The χ^2-test gives a confidence interval for each varying parameter, e.g. where the probability is 68.3 %, 95 % or 99 % that the true value is within the calculated value. A confidence interval can be plotted as a contour around a *confidence region* of a certain probability of finding the true parameter value. In a χ^2 distribution with two fitted parameters the following confidence regions are given in [4]

Probability	Confidence region
68.3 %	$\chi^2 = \chi^2_{min}$+2.30
95 %	$\chi^2 = \chi^2_{min}$+5.99
99 %	$\chi^2 = \chi^2_{min}$+9.21

4.1.2 Constraints

In some χ^2-tests degeneracy appears in parameter space. For instance, when dividing the time delay differences the confidence regions in Ω_M-η space becomes very elongated. One way to remove or at least mitigate these degeneracies can be done by applying constraints or priors on the parameter, i.e. one can impose or assume a prior knowledge [29] [9].

Thus, if we have prior knowledge of Ω_M the degeneracy can be removed or mitigated by [9]

$$\chi^2 = \chi^2_0 + \frac{(\Omega_M - \Omega_{M_{prior}})^2}{\sigma^2_{prior}} \tag{74}$$

where χ^2_0 denotes the χ^2 without prior knowledge of Ω_M, and σ_{prior} is the uncertainty in $\Omega_{M_{prior}}$.

4.2 Observables

Since a change in a DOL-system's redshifts and velocity dispersion affects the image angles and the time delays, the observables are depending on each other. The subsections below explains how my observables are chosen and how the flux can be used to improve the parameter estimations.

4.2.1 Image angles

When the time delay function for a power law lens, eq. (70), was derived, the assumption was made that $\Delta\zeta/\langle\zeta\rangle$ is small. The image angles are then depending on this assumption as

$$\frac{\Delta\zeta}{\langle\zeta\rangle} = 2\,\frac{\theta_1 - \theta_2}{\theta_1 + \theta_2} < 1 \tag{75}$$

For a SIS-lens producing two source images at the angles θ_1 and θ_2, appendix C show that

$$\theta_E = \frac{\theta_1 + \theta_2}{2} \tag{76}$$

where θ_E is given by eq. (62).

Now, combining eq. (75) and eq. (76) gives

$$\begin{cases} \theta_1 < \frac{3}{2}\,\theta_E, \\ \theta_2 > \frac{1}{2}\,\theta_E \end{cases} \tag{77}$$

which will limit my simulated image angles. Note that larger image angle differences could be simulated by not making the assumption in eq. (70) (results from the simulations shows that larger image separations improves the parameter estimations).

By simulating DOL-systems with different z_i and σ_v, the image angles are calculated by using the eqs. (61), (62), (76) and (77). These angle values are then considered as the observed image angles.

To get useful time delays for my parameter estimations the light path differences between the images must be significant. Therefore, I simulate the observed image angles at the limit of eq. (77), which gives

$$\begin{cases} \theta_{a_1} = & 1.49\,\theta_E \\ \theta_{a_2} = & 0.51\,\theta_E \\ \theta_{b_1} = & 1.49\,\theta_E \\ \theta_{b_2} = & 0.51\,\theta_E \end{cases} \tag{78}$$

Appendix D show that the image magnification for a SIS-lens is dependent on the image angle and on θ_E. By using the chosen values from eq. (78) the magnification for each image from a lensed source becomes

$$\begin{cases} \theta_1 = & 1.49\,\theta_E & \Longrightarrow & \mu_1 = \left|\frac{\theta_1}{\theta_1 - \theta_E}\right| \approx 3 \\ \theta_2 = & 0.51\,\theta_E & \Longrightarrow & \mu_2 = \left|\frac{\theta_2}{\theta_E - \theta_2}\right| \approx 1 \end{cases} \tag{79}$$

Therefore, in all simulations, the energy flux from θ_{a_1} and θ_{b_1} becomes three times larger than from their sources, and unchanged from θ_{a_2} and θ_{b_2}.

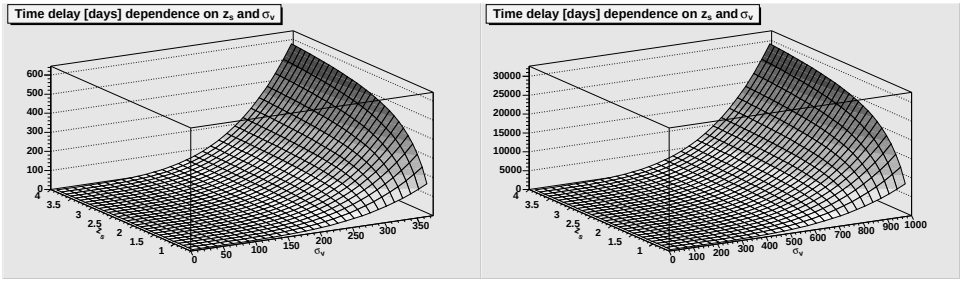

Figure 7: SIS time delay dependence in days on z_s, and σ_v for a lens at redshift $z_l = 0.5$ and $\Omega_M = 0.3$ in a flat universe.

4.2.2 Measuring Time Delays

Time delays are hard to measure if the fluxes from the images are not time varying, or if the images are faint or if they lie to close to each other [14]. Therefore, gravitational lensed galaxies are not good sources for time delay studies, better sources for measuring time delays are quasars and supernovae.

The first time delay measurement was made 1984 [7], in the double quasar QSO 0957+561A, B. The basic procedure for measuring a time delay is that an observation must produce light curves for the individual lensed images that are well sampled compared to the time delays, and that during this period the lensed source have brightness fluctuations of time scales shorter than the this period [14].

The properties of the lens determines the time delay. For instance, the more massive the lens, the longer the time delay. The time delays are also affected by the profile of lens, its ellipticity, surrounding massive satellite galaxies and if it is a member of a cluster; the cluster surface density at the position of the lens [14] [31].

In my simulations the velocity dispersion is chosen just enough to make time delays about a few years. Fig. (7) shows how the SIS time delay depends on the redshift of the source z_s and σ_v in a lens at redshift $z_l = 0.5$ and $\Omega_M = 0.3$ in a flat universe.

4.2.3 Redshift Proportions

To find where the simulated redshift proportions in a DOL-system gives the best parameter estimations, I made a program calculating for which z_l Ω_M has the smallest 68.3 % confidence interval for fixed z_a and z_b.

4.2.4 Flux Ratio

The *flux ratio* for a lensed object in a DOL-system is given by [17]

$$r \equiv \frac{\mu_1}{|\mu_2|} \tag{80}$$

where μ_i is defined in eq. (49). After some calculations using eq. (49) in eq. (80), the flux ratio from a power law lens can be expressed as

$$\begin{aligned} r_{pow} &= \left|\frac{\theta_1}{\theta_2}\right| \left|\frac{1-(2-\eta)\,\theta_2^{1-\eta}\,(\theta_1+\theta_2)\,/\,(\theta_1^{2-\eta}+\theta_2^{2-\eta})}{1-(2-\eta)\,\theta_1^{1-\eta}\,(\theta_1+\theta_2)\,/\,(\theta_1^{2-\eta}+\theta_2^{2-\eta})}\right| = \\ &= r_{sis}\left|\frac{1-(2-\eta)\,\theta_2^{1-\eta}\,(\theta_1+\theta_2)\,/\,(\theta_1^{2-\eta}+\theta_2^{2-\eta})}{1-(2-\eta)\,\theta_1^{1-\eta}\,(\theta_1+\theta_2)\,/\,(\theta_1^{2-\eta}+\theta_2^{2-\eta})}\right| = \\ &= r_{sis}\cdot r_{chi} \end{aligned} \tag{81}$$

where

$$r_{sis} = \left|\frac{\theta_1}{\theta_2}\right| \tag{82}$$

and

$$r_{chi} = \left|\frac{1-(2-\eta)\,\theta_2^{1-\eta}\,(\theta_1+\theta_2)\,/\,(\theta_1^{2-\eta}+\theta_2^{2-\eta})}{1-(2-\eta)\,\theta_1^{1-\eta}\,(\theta_1+\theta_2)\,/\,(\theta_1^{2-\eta}+\theta_2^{2-\eta})}\right|. \tag{83}$$

In appendix E the r_i-expressions are calculated.

Thus, by using the flux ratios from a DOL-system one can estimate η alone with no information needed about the cosmology.

The uncertainties in the flux ratios are dominated by the effects of microlensing by compact objects and millilensing by cold dark matter, rather than from flux measurement uncertainties [17]. Mörtsell, Dahl and Hannestad (2004) [17] estimates this uncertainty as $\sigma_{obs} = f_{obs}\, r_{obs} = 0.5\, r_{obs}$, where f_{obs} depends on the micro- and millilensing mentioned above. Therefore, σ_{th} can be neglected and the χ^2-test for the flux ratio becomes

$$\chi^2 = \sum\left(\frac{r_{th}(\eta,\theta_1,\theta_2) - r_{obs}}{f_{obs}\, r_{obs}}\right)^2 = \sum\left(\frac{r_{chi}(\eta,\theta_1,\theta_2) - 1}{f_{obs}}\right)^2 \tag{84}$$

where as before $_{obs}$ denotes the simulated value (using the SIS lens model) and $_{th}$ denotes the theoretical value (using the power law lens model).

4.3 Different Types of Estimations

In every simulation I will run two different types of estimations; one where the values of Ω_M and η are investigated by taking the quotient between the time delay differences of two lensed objects (in this case the H_0 parameter disappears), and another where the values of H_0, Ω_M and η are investigated by summing the χ^2 values for each lensed object. In each type of estimation the χ^2 expressions takes different forms.

4.3.1 Expression for the Power Law Quotient

In a DOL-system with two lensed sources a and b each producing two images, the power law time delay quotient between the sources becomes

$$q_{pow} = D_q \left[\frac{\theta_{a_1}^2 - \theta_{a_2}^2}{\theta_{b_1}^2 - \theta_{b_2}^2}\right] \left[\frac{3-(2-\eta)^2\left(1-\frac{2\theta_{a_2}}{\theta_{a_1}+\theta_{a_2}}\right)^2}{3-(2-\eta)^2\left(1-\frac{2\theta_{b_2}}{\theta_{b_1}+\theta_{b_2}}\right)^2}\right] \tag{85}$$

where

$$D_q = \frac{D_a\, D_{lb}}{D_b\, D_{la}} \tag{86}$$

which according to eq. (35) is given by

$$D_q = \frac{\int_{z_0}^{z_a} \frac{d\acute{z}}{[\Omega_M((1+\acute{z})^3-1)+1]^{1/2}} \left[\int_{z_0}^{z_b} \frac{d\acute{z}}{[\Omega_M((1+\acute{z})^3-1)+1]^{1/2}} - \int_{z_0}^{z_l} \frac{d\acute{z}}{[\Omega_M((1+\acute{z})^3-1)+1]^{1/2}}\right]}{\int_{z_0}^{z_b} \frac{d\acute{z}}{[\Omega_M((1+\acute{z})^3-1)+1]^{1/2}} \left[\int_{z_0}^{z_a} \frac{d\acute{z}}{[\Omega_M((1+\acute{z})^3-1)+1]^{1/2}} - \int_{z_0}^{z_l} \frac{d\acute{z}}{[\Omega_M((1+\acute{z})^3-1)+1]^{1/2}}\right]}. \tag{87}$$

Thus, dividing the time delays kills the Hubble parameter and only two parameters remains, Ω_M and η.

Since the flux ratio eq. (81) is sensitive to η and not to Ω_M, the flux ratios can be added to the χ^2-test and act like a prior for η. For i number of sources and j number of varying parameters, the χ^2 takes the form

$$\boldsymbol{\chi^2} = \begin{pmatrix} \chi^2(\Omega_{M_1}, \eta_1) & \cdots & \chi^2(\Omega_{M_j}, \eta_1) \\ \vdots & \ddots & \vdots \\ \chi^2(\Omega_{M_1}, \eta_j) & \cdots & \chi^2(\Omega_{M_j}, \eta_j) \end{pmatrix}, \tag{88}$$

where

$$\chi^2(\Omega_M, \eta) = \frac{(q_{th} - q_{obs})^2}{\sigma_{q_{th}}^2 + \sigma_{q_{obs}}^2} + \sum_i \left(\frac{r_{chi_i} - 1}{f_{obs}}\right)^2, \tag{89}$$

where $q_{obs} = \Delta t_{a_{obs}}/\Delta t_{b_{obs}}$ and $\sigma_{q_{obs}}$ is the propagation in q_{obs} given by

$$\sigma_{q_{obs}} = \left[\left(\frac{\partial q_{obs}}{\partial \Delta t_{a_{obs}}}\,\delta_{t_{a_{obs}}}\right)^2 + \left(\frac{\partial q_{obs}}{\partial \Delta t_{b_{obs}}}\,\delta_{t_{b_{obs}}}\right)^2\right]^{1/2} = q_{obs}\left[\frac{\delta_{t_{a_{obs}}}^2}{\Delta t_{a_{obs}}^2} + \frac{\delta_{t_{b_{obs}}}^2}{\Delta t_{b_{obs}}^2}\right]^{1/2}. \tag{90}$$

Without any covariance among the observables the uncertainty $\sigma_{q_{th}}$ becomes

$$\begin{aligned} \sigma_{q_{th}} \;=\; & \left[\left(\frac{\partial q}{\partial \theta_{a_1}}\,\delta_{\theta_{a_1}}\right)^2 + \left(\frac{\partial q}{\partial \theta_{a_2}}\,\delta_{\theta_{a_2}}\right)^2 + \left(\frac{\partial q}{\partial \theta_{b_1}}\,\delta_{\theta_{b_1}}\right)^2 + \left(\frac{\partial q}{\partial \theta_{b_2}}\,\delta_{\theta_{b_2}}\right)^2 + \right. \\ & \left. + \left(\frac{\partial q}{\partial z_a}\,\delta_{z_a}\right)^2 + \left(\frac{\partial q}{\partial z_b}\,\delta_{z_b}\right)^2 + \left(\frac{\partial q}{\partial z_l}\,\delta_{z_l}\right)^2\right]^{1/2}. \end{aligned} \tag{91}$$

In appendix F the expression for $\sigma_{q_{th}}$ is calculated.

4.3.2 Expression for Summing χ^2

When summing χ^2 for a DOL-system the time delay is $\Delta t_i(\Omega_M, H_0, \eta)$, so all parameters remains. In the contour plots I will use a fixed value for η and then perturb it to see how the perturbation affects the estimation of Ω_M and H_0.

Therefore, for i number of sources and j number of varying parameter values, the total χ^2 takes the form

$$\chi^{\mathbf{2}} = \begin{pmatrix} \chi^2(\Omega_{M_1}, H_{0_1}) & \dots & \chi^2(\Omega_{M_j}, H_{0_1}) \\ \vdots & \ddots & \vdots \\ \chi^2(\Omega_{M_1}, H_{0_j}) & \dots & \chi^2(\Omega_{M_j}, H_{0_j}) \end{pmatrix}, \tag{92}$$

where

$$\chi^2(\Omega_M, H_0) = \sum_i \frac{(\Delta t_i - \Delta t_{i_{obs}})^2}{\sigma_i^2 + \sigma_{i_{obs}}^2} \tag{93}$$

where Δt_i and $\Delta t_{i_{obs}}$ are given by eq. (70) respective eq. (65), the uncertainties σ_i are propagated without any covariance as

$$\sigma_{i_{th}} = \left[\left(\frac{\partial \Delta t}{\partial \theta_{i_1}} \delta\theta_{i_1} \right)^2 + \left(\frac{\partial \Delta t}{\partial \theta_{i_2}} \delta\theta_{i_2} \right)^2 + \left(\frac{\partial \Delta t}{\partial z_i} \delta z_i \right)^2 + \left(\frac{\partial \Delta t}{\partial z_l} \delta z_l \right)^2 + \left(\frac{\partial \Delta t}{\partial \eta} \delta_\eta \right)^2 \right]^{1/2}. \tag{94}$$

In appendix G the expression for σ_{th} is calculated.

4.4 Uncertainties

In the χ^2-expression, eq. (73), the uncertainties are σ_{obs} and σ_{th}, where the later takes different forms depending on estimation type. When running my estimations the contribution from δ_{z_i} in the eq. (91) becomes very small compared to the contribution from δ_{θ_i}, using $\delta_{z_i} = 0.001$ [11]. Therefore, the quotient parameter estimations are affected by the measurement errors from the observed image angles and the observed time delay. The domination of δ_{θ_i} in eq. (91) can be understood if one thinks about how an error in the angle measurements can make the geometrical light path significantly longer or shorter.

The uncertainty δ_t from lensed quasars can be estimated from current SIS time delay observations, e.g. [14] or [31]. In the simulations, δ_t from a lensed quasar is estimated as $\delta_t = 2.0$ [days].

Mörtsell, Dahle and Hannestad (2004) [17] estimates $\delta_t = 0.15$ [days] when using the future Supernova Acceleration Probe (SNAP), which makes this σ_{obs} only valid when observing supernovae.

The uncertainty in the image angles are estimated in Goobar *et al.* (2002) [11] as $\delta_{\theta_i} = 0.01''$.

Anderson and King (2000) [1] reports that, having a rich star field their Point Spread Function can measure the position of a bright star with a

precision of $0.002''$, which is the used uncertainty in my most extreme simulations.

In the flux ratio estimation, eq. (84), $f_{obs} = 0.5$ [17] is used.

4.5 Sub-simulations

Due to the uncertainty in determining the observed uncertainties and their domination in the quotient estimations, I make four sub-simulations with different values of δ_{θ_i} and δ_t.

In the sub-simulation called *quasar*, two quasars are lensed in a DOL-system with the uncertainties

$$\begin{cases} \delta_{\theta_i} &= 0.01 \quad \text{[arcsec]} \\ \delta_t &= 2.0 \quad \text{[days]}. \end{cases} \tag{95}$$

In the sub-simulation called *nova-quasar*, one quasar and one supernova are lensed in a DOL-system with the uncertainties

$$\begin{cases} \delta_{\theta_i} &= 0.01 \quad \text{[arcsec]} \\ \delta_{t_{SNe}} &= 0.15 \quad \text{[days]} \\ \delta_{t_{QSO}} &= 2.0 \quad \text{[days]} \end{cases} \tag{96}$$

where $\delta_{t_{SNe}} = 0.15$ and $\delta_{t_{QSO}} = 2.0$ are the time uncertainty from a supernova respective a quasar. Since eq. (90) gives smaller σ_{obs} when $\delta_{t_b} > \delta_{t_a}$, source a is a supernova and source b is a quasar in all nova-quasar sub-simulations.

In the sub-simulation *supernova*, two supernovae are lensed in a DOL-system with the uncertainties

$$\begin{cases} \delta_{\theta_i} &= 0.01 \quad \text{[arcsec]} \\ \delta_t &= 0.15 \quad \text{[days]}. \end{cases} \tag{97}$$

In the sub-simulation *extreme-supernova*, two supernovae are lensed in a DOL-system with the uncertainties

$$\begin{cases} \delta_{\theta_i} &= 0.002 \quad \text{[arcsec]} \\ \delta_t &= 0.15 \quad \text{[days]}. \end{cases} \tag{98}$$

Since the uncertainty δ_η dominates in the summing χ^2-estimations, the uncertainties from δ_{θ_i} and δ_t becomes less important. Instead, I make one sub-simulation where $\eta = 2.0$ and another where $\eta = 1.5$, in both cases we have $\delta_{\theta_i} = 0.01$ and $\delta_t = 2.0$.

5 Results

I simulate five DOL-systems with different observables for calculating time delays which then are used to estimate Ω_M, η and H_0 with different types of χ^2-tests. The observed image angles are calculated by eq. (78), and the observed time delays are calculated by using eq. (65) with the assumed values for Ω_M and H_0 from eq. (71). Since the time delays are very sensitive to the mass of the lens, the velocity dispersions are chosen not to make up too long time delays. In all simulations I assume a flat universe, i.e. $k = 0$, thus the angular distances are given by eq. (35).

In the five sections below, the results from each simulation are given in figures and tables, which contents are more explained in detail in section 5.1.

All my computer programs are made in `C++`, but in a ordinary `C++` package there are no codes for making nice plots and more advanced calculations (as far as I know...). However, by using the `C++` package `ROOT` which contains lots of mathematically tools, almost everything can be programed in `C++`. `ROOT` has been developed in Cern and was first publicly released in the end of 1995[12].

5.1 Simulation A

In simulation A, a DOL-system is simulated with the observables

$$\begin{cases} z_l &= 0.55 \pm 0.001 \\ z_a &= 1.0 \pm 0.001 \\ z_b &= 2.0 \pm 0.001 \\ \sigma_v &= 375 \quad [\text{km s}^{-1}] \end{cases} \tag{99}$$

Using eq. (76) the image angles becomes

$$\begin{cases} \theta_{a_1} &= 2.29 \quad [\text{arcsec}] \\ \theta_{a_2} &= 0.79 \quad [\text{arcsec}] \\ \theta_{b_1} &= 3.65 \quad [\text{arcsec}] \\ \theta_{b_2} &= 1.25 \quad [\text{arcsec}] \end{cases} \Longrightarrow \begin{cases} \theta_{E_a} &= 1.54 \quad [\text{arcsec}] \\ \theta_{E_b} &= 2.45 \quad [\text{arcsec}] \end{cases} \tag{100}$$

Using these θ-values and $\Omega_M = 0.30 \pm 0.04$, the SIS time delay for each source (eq. (65)) and the quotient between them becomes

$$\begin{cases} \Delta t_a &= 351 \quad [\text{days}] \\ \Delta t_b &= 559 \quad [\text{days}] \end{cases} \Longrightarrow q_{sim} = \begin{cases} 0.628 \pm 0.004 & ,\text{quasar} \\ 0.628 \pm 0.002 & ,\text{nova-quasar} \\ 0.628 \pm 0.0003 & ,\text{supernova} \end{cases} \tag{101}$$

where the quotient uncertainties are the error propagations in $\Delta t_a / \Delta t_b$ for each sub-simulation[13].

[12] More information can be found at `http://root.cern.ch/root`.

[13] The same uncertainty is given in the sub-simulation supernova and extreme-supernova since the δ_t's are the same

5.1.1 Simulation A - Time Delay Quotient

In simulation A the χ^2-tests from the time delay quotients and the flux ratios estimates the contour regions as Fig. (8) and (9), which gives the following values for Ω_M and η

Estimation	Probability	Ω_M	η	σ_{th}
Flux	68.3 %	—	$2.00^{+0.35}_{-0.52}$	—
	95 %	—	$2.00^{+0.53}_{-1.05}$	
	99 %	—	$2.00^{+0.64}$	
quasar	68.3 %	$0.30^{+0.64}$	$2.00^{+0.35}_{-0.52}$	$\sigma_{th} = 3\,\sigma_{obs}$
	95 %	—	$2.00^{+0.53}_{-1.05}$	
	99 %	—	$2.00^{+0.64}$	
nova-quasar	68.3 %	$0.30^{+0.57}$	$2.00^{+0.35}_{-0.52}$	$\sigma_{th} = 10\,\sigma_{obs}$
	95 %	—	$2.00^{+0.53}_{-1.05}$	
	99 %	—	$2.00^{+0.64}$	
super-nova	68.3 %	$0.30^{+0.55}$	$2.00^{+0.35}_{-0.52}$	$\sigma_{th} = 500\,\sigma_{obs}$
	95 %	—	$2.00^{+0.53}_{-1.05}$	
	99 %	—	$2.00^{+0.64}$	
extreme super-nova	68.3 %	$0.30^{+0.09}_{-0.10}$	$2.00^{+0.35}_{-0.52}$	$\sigma_{th} = 20\,\sigma_{obs}$
	95 %	$0.30^{+0.15}_{-0.29}$	$2.00^{+0.53}_{-1.05}$	
	99 %	$0.30^{+0.19}$	$2.00^{+0.64}$	

The Flux Ratio-row is the results from the flux ratio estimation alone, which becomes the same in all sub-simulations. The quasar-row is the combined results from the flux ratio and the time delay quotient estimations in the quasar sub-simulation, the nova-quasar-row is the combined results from nova-quasar the sub-simulation, the supernova-row is the combined results from the supernova sub-simulation and the extreme-supernova-row is the combined results from the extreme supernova sub-simulation. The σ_{th}-column gives the relations between the uncertainties σ_{th} and σ_{obs} in each sub-simulation.

Since the estimations with a $\Omega_{M-prior}$ give the same η values as the other estimations and since Ω_M never is estimated when using a $\Omega_{M-prior}$, the parameter values from these estimations are not given in the table.

The lines in the table marks where no estimation could be obtained, and in some estimations no lower confidence interval could be estimated.

Due to the degeneracy that appears from the extreme-supernova time delay quotient estimation, the Ω_M value for 68.3 % corresponds to the right confidence region in fig. (9).

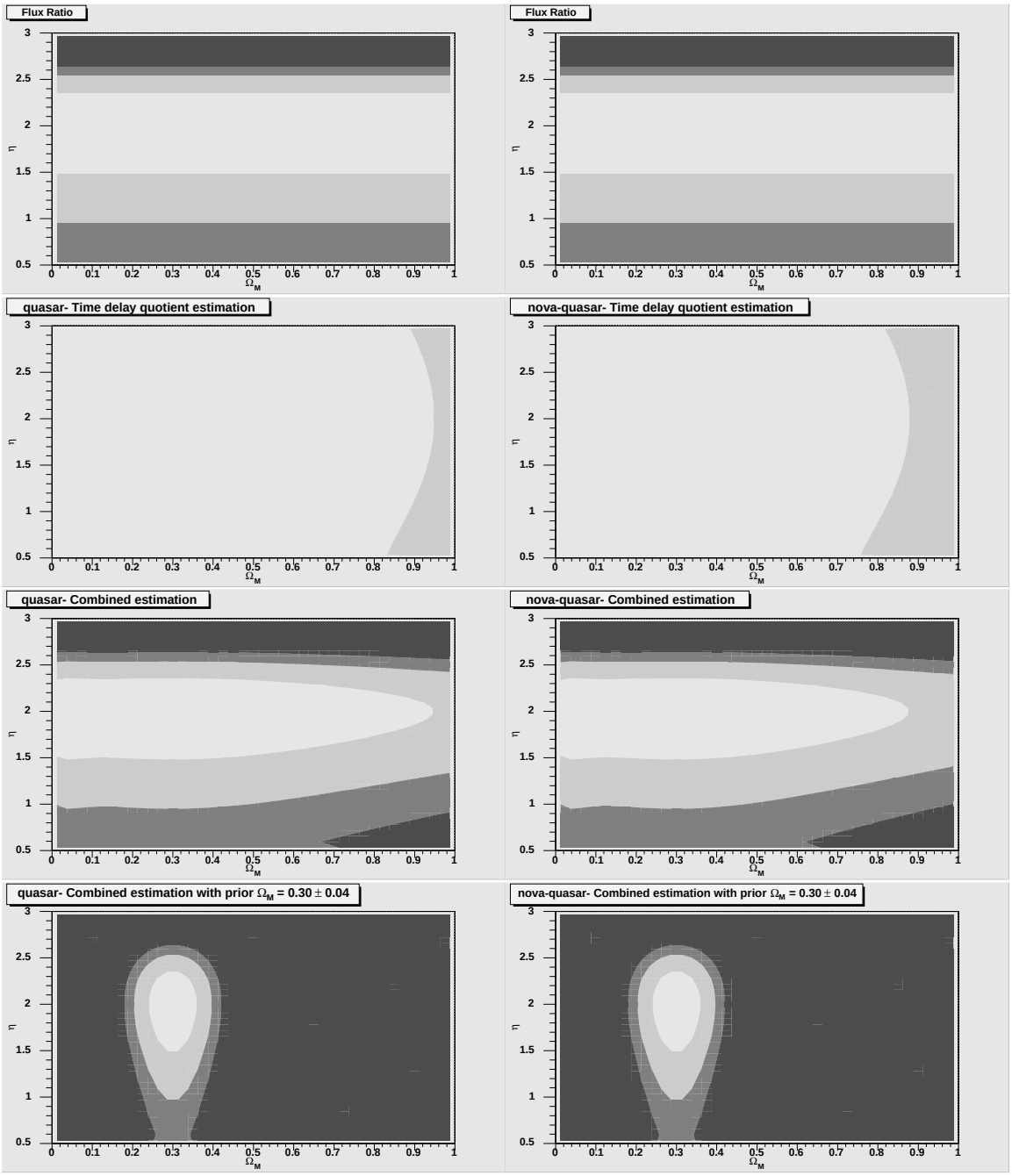

Figure 8: quasar and nova-quasar time delay quotient estimations from simulation A. The upper row shows the estimations from the flux ratio, the second row shows the time delay quotient estimations, the third row shows the combined estimations and the lowest row shows the combined estimations using a prior on Ω_M. The 68.3 % confidence interval is within the white area, the 95 % is within the white-grey area and the 99 % is within the grey-black area.

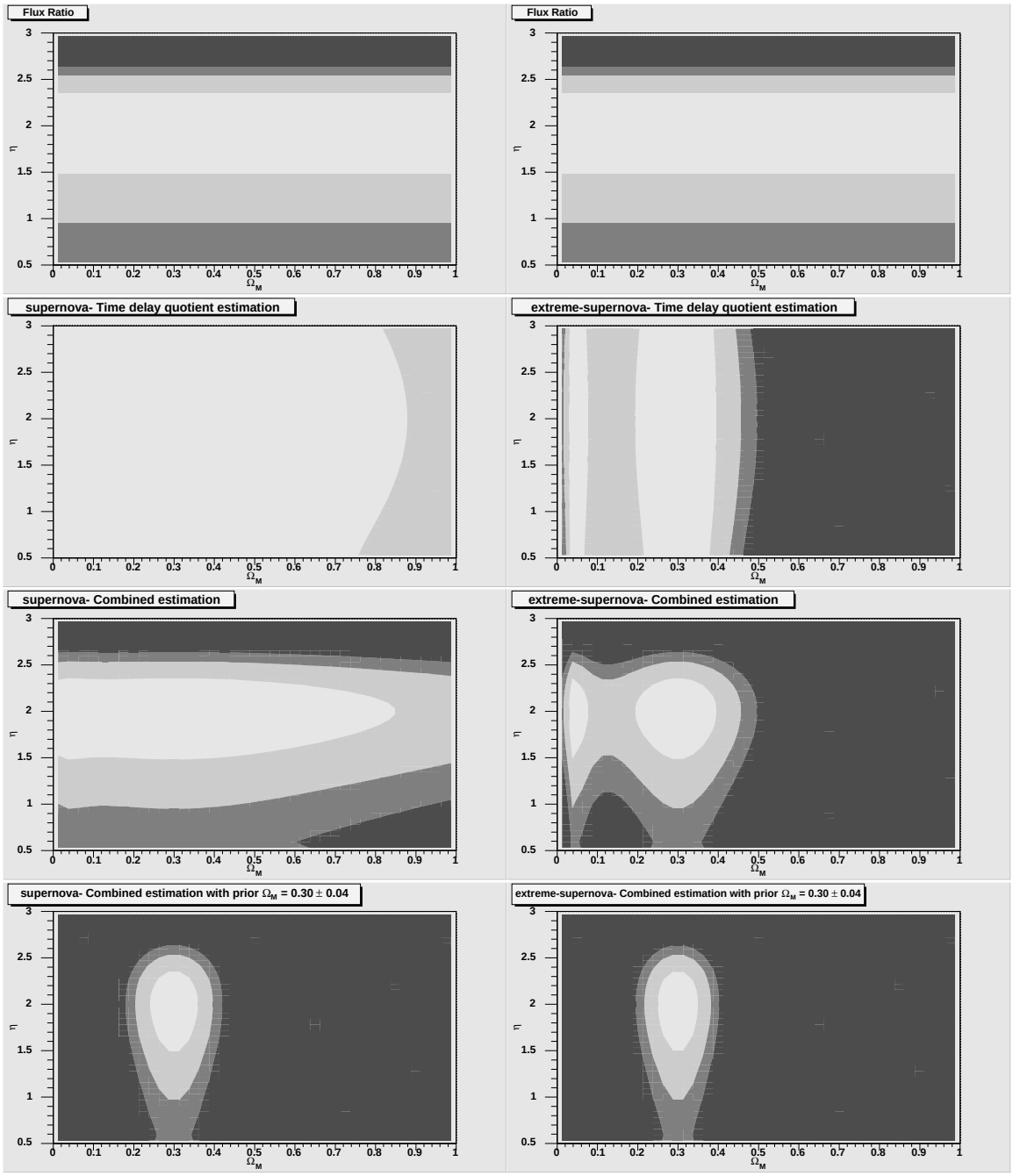

Figure 9: supernova and extreme-supernova time delay quotient estimations from simulation A. The upper row shows the estimations from the flux ratio, the second row shows the time delay quotient estimations, the third row shows the combined estimations and the lowest row shows the combined estimation using a prior on Ω_M. The 68.3 % confidence interval is within the white area, the 95 % is within the white-grey area and the 99 % is within the grey-black area.

5.1.2 Simulation A -Summing χ^2 in H_0-Ω_M Space

In simulation A the summing χ^2 in H_0-Ω_M space gives the contour regions as Fig. (10), where the two figure columns shows how dominant the value of η becomes. In the left column $\eta = 2.0$ and in right column $\eta = 1.5$. When using $\delta_\theta = 0.01''$, $\delta_t = 2.0$ [days] and $\delta_\eta = 0.1$ the uncertainty from $\left(\frac{\partial \Delta t}{\partial \eta}\,\delta_\eta\right)$ becomes about 100 times larger than σ_{obs}, eq. (93).

Figure (10) shows that the summing χ^2-estimations gives no information of Ω_M and only H_0 can be estimated. The estimated values of H_0 are

A	Probability	Source A	Source B	Sum of χ^2	$\Omega_{M-prior}$
H_0	68.3 %	67^{+14}_{-10}	66^{+15}_{-11}	69^{+9}_{-10}	70^{+8}_{-7}
	95 %	67^{+21}_{-16}	66^{+21}_{-17}	69^{+13}_{-15}	70^{+12}_{-12}
	99 %	67^{+24}_{-21}	66^{+25}_{-20}	69^{+16}_{-17}	70^{+15}_{-15}

where Source A-column are the results from source A alone, Source B-column is source B alone, Sum of χ^2-column are the combined results, and the $\Omega_{M-prior}$-column are the combined results when using a prior $\Omega_M = 0.30 \pm 0.04$.

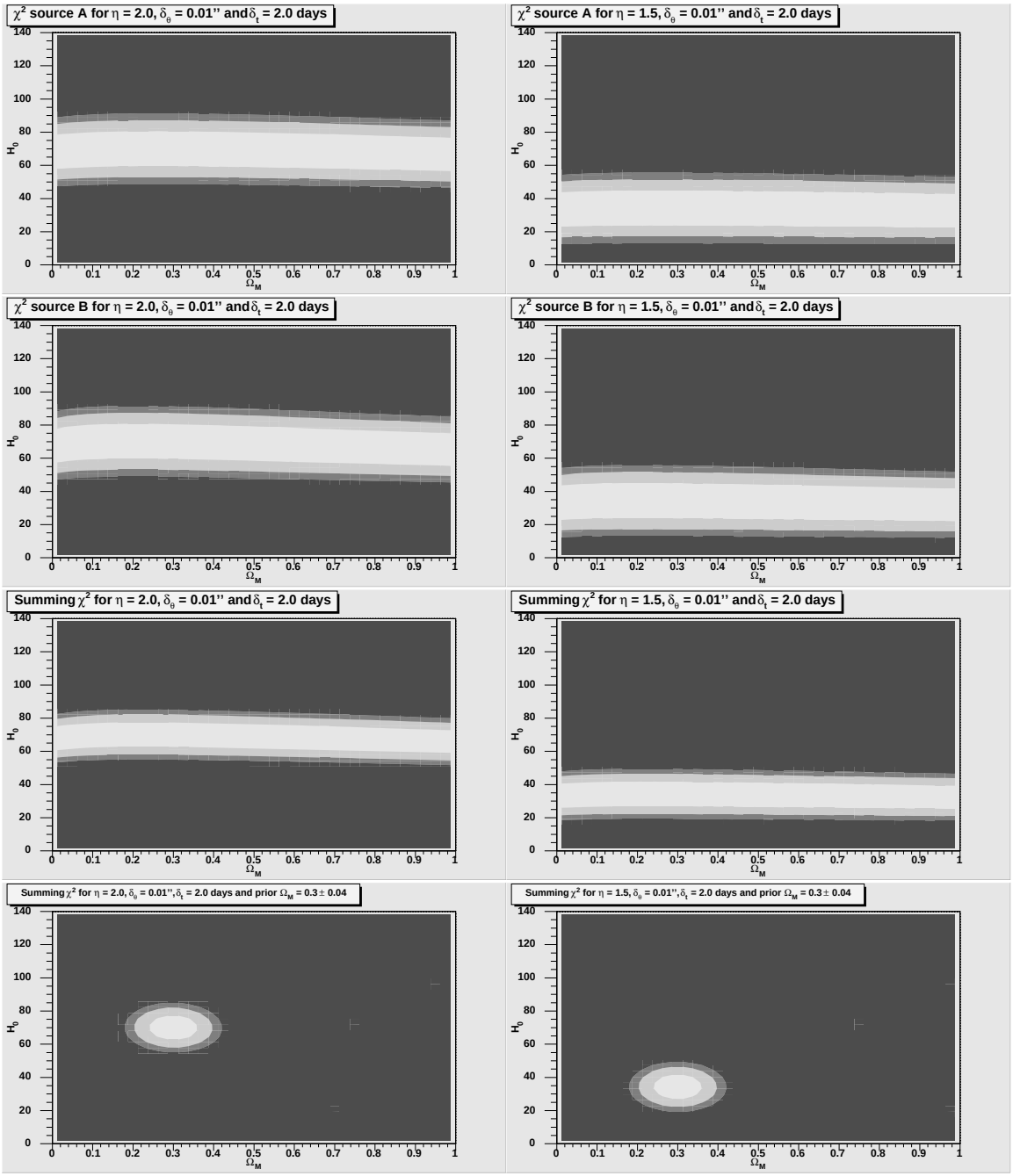

Figure 10: Summing χ^2 from simulation A. The left column shows estimations for $\eta = 2.0$ and the right shows estimations for $\eta = 1.5$, in both cases are $\delta_\theta = 0.01''$ and $\delta_t = 2.0$ [days]. From above, the first row shows estimations for source A alone, the second row shows estimations for source B alone, the third row shows estimations of the sum of χ^2 and the lowest row shows estimations of the sum of χ^2 with a $\Omega_{M-prior} = 0.30 \pm 0.04$. The 68.3 % confidence interval is within the white area, the 95 % is within the white-grey area and the 99 % is within the grey-black area.

5.2 Simulation B

In simulation B, a DOL-system is simulated with the observables

$$\begin{cases} z_l &= 0.4 \pm 0.001 \\ z_a &= 0.75 \pm 0.001 \\ z_b &= 1.0 \pm 0.001 \\ \sigma_v &= 375 \quad [\text{km s}^{-1}] \end{cases} \tag{102}$$

Using eq. (76) the image angles becomes

$$\begin{cases} \theta_{a_1} &= 2.50 \quad [\text{arcsec}] \\ \theta_{a_2} &= 0.86 \quad [\text{arcsec}] \\ \theta_{b_1} &= 3.21 \quad [\text{arcsec}] \\ \theta_{b_2} &= 1.10 \quad [\text{arcsec}] \end{cases} \Longrightarrow \begin{cases} \theta_{E_a} &= 1.68 \quad [\text{arcsec}] \\ \theta_{E_b} &= 2.15 \quad [\text{arcsec}] \end{cases} \tag{103}$$

Using these θ-values and $\Omega_M = 0.30 \pm 0.04$, the SIS time delay for each source (eq. (65)) and the quotient between them becomes

$$\begin{cases} \Delta t_a &= 290 \quad [\text{days}] \\ \Delta t_b &= 371 \quad [\text{days}] \end{cases} \Longrightarrow q_{sim} = \begin{cases} 0.781 \pm 0.007 & \text{, quasar} \\ 0.781 \pm 0.004 & \text{, nova-quasar} \\ 0.781 \pm 0.0005 & \text{, supernova} \end{cases} \tag{104}$$

5.2.1 Simulation B - Time Delay Quotient

In simulation B the χ^2-tests from the time delay quotients and the flux ratios gives the contour regions as Fig. (11) and (12), which gives the following values for Ω_M and η

Estimation	Probability	Ω_M	η	σ_{th}
Flux	68.3 %	—	$2.00^{+0.35}_{-0.52}$	—
	95 %	—	$2.00^{+0.53}_{-1.05}$	
	99 %	—	$2.00^{+0.64}$	
quasar	68.3 %	—	$2.00^{+0.35}_{-0.52}$	$\sigma_{th} = 2\,\sigma_{obs}$
	95 %	—	$2.00^{+0.53}_{-1.05}$	
	99 %	—	$2.00^{+0.64}$	
nova-quasar	68.3 %	—	$2.00^{+0.35}_{-0.52}$	$\sigma_{th} = 4\,\sigma_{obs}$
	95 %	—	$2.00^{+0.53}_{-1.05}$	
	99 %	—	$2.00^{+0.64}$	
super-nova	68.3 %	—	$2.00^{+0.35}_{-0.52}$	$\sigma_{th} = 300\,\sigma_{obs}$
	95 %	—	$2.00^{+0.53}_{-1.05}$	
	99 %	—	$2.00^{+0.64}$	
extreme super-nova	68.3 %	$0.30^{+0.38}$	$2.00^{+0.35}_{-0.52}$	$\sigma_{th} = 10\,\sigma_{obs}$
	95 %	$0.30^{+0.61}$	$2.00^{+0.53}_{-1.05}$	
	99 %	—	$2.00^{+0.64}$	

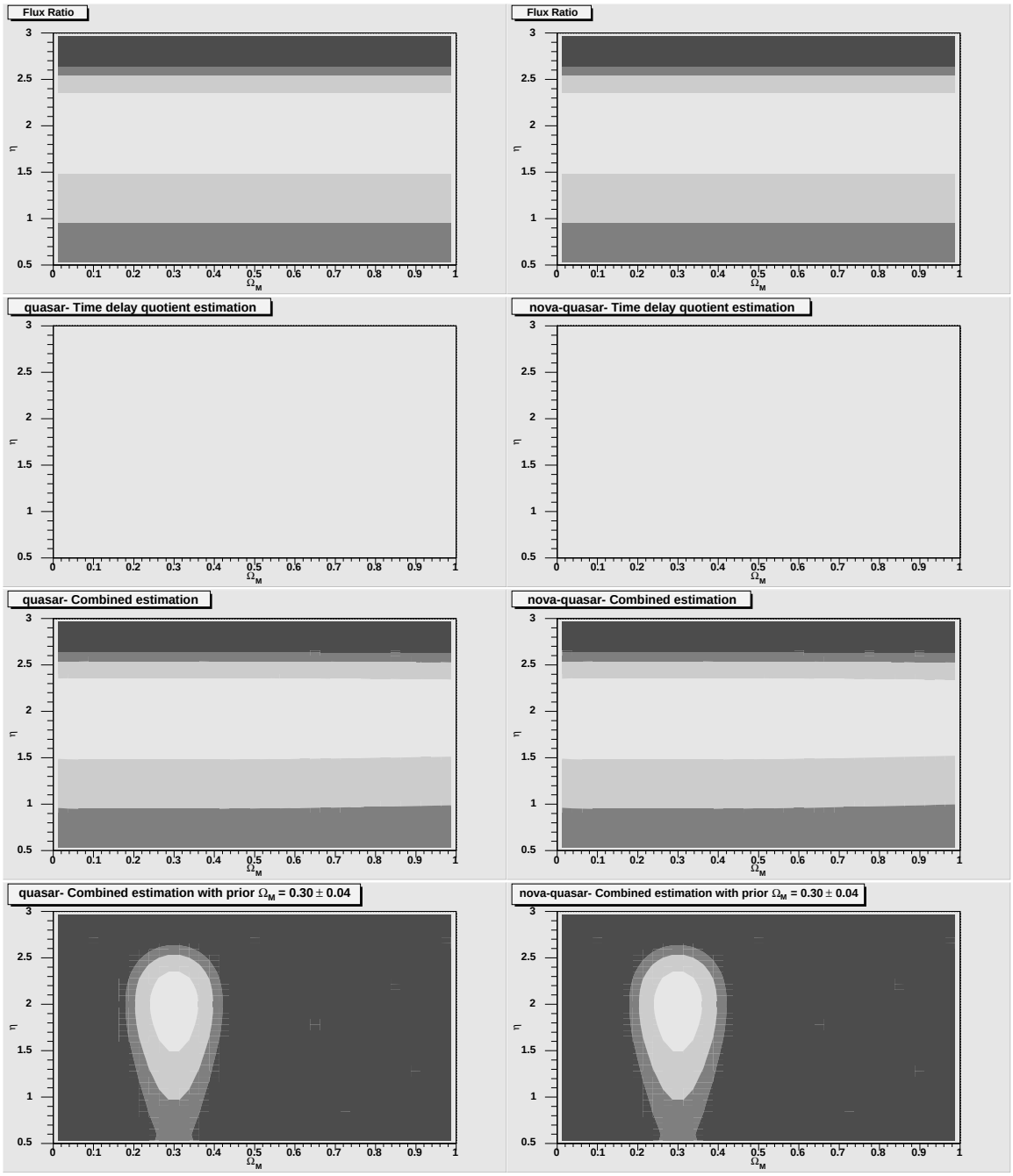

Figure 11: quasar and nova-quasar time delay quotient estimations from simulation B. The upper row shows the estimations from the flux ratio, the second row shows the time delay quotient estimations, the third row shows the combined estimations and the lowest row shows the combined estimations using a prior on Ω_M. The 68.3 % confidence interval is within the white area, the 95 % is within the white-grey area and the 99 % is within the grey-black area.

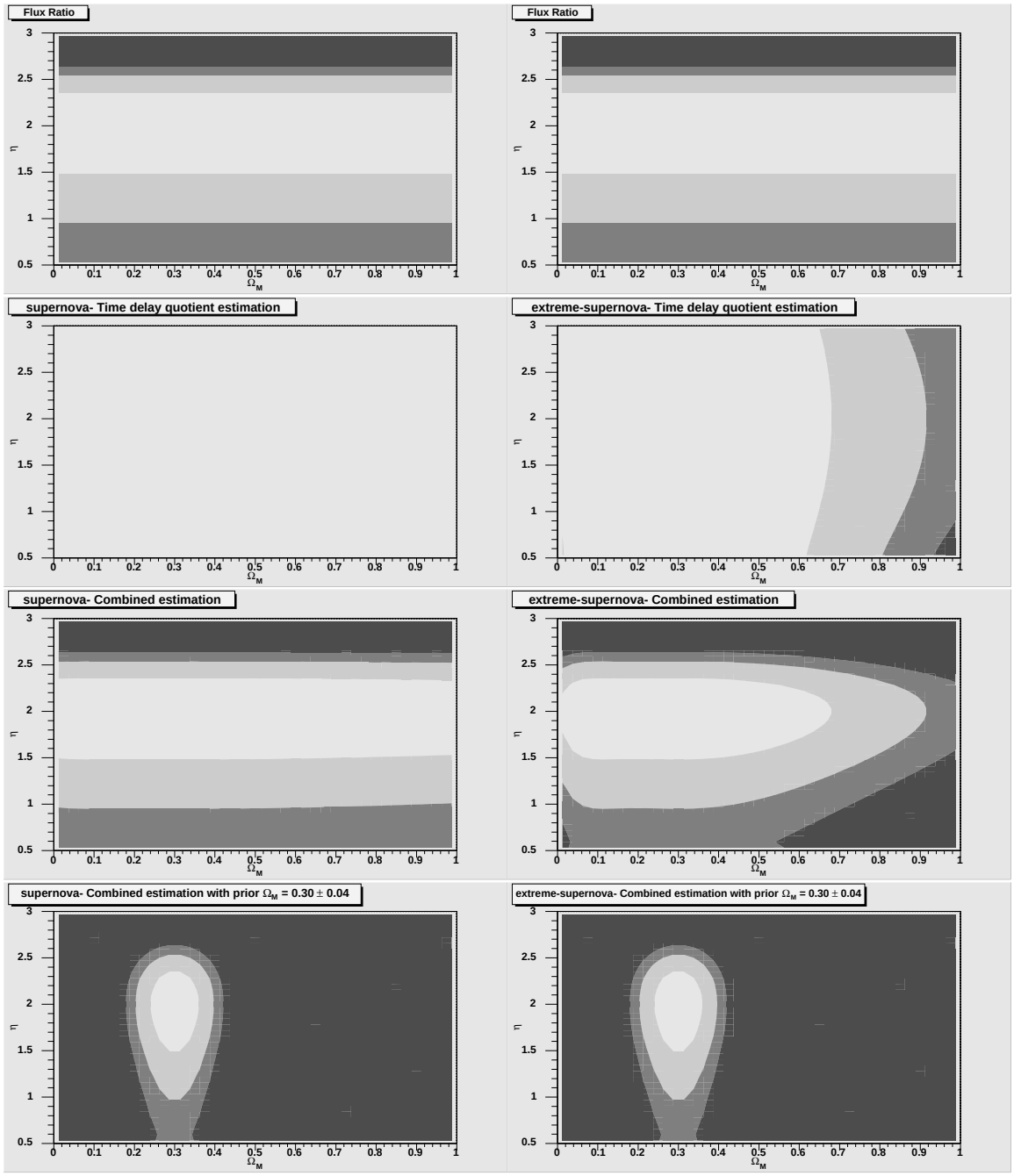

Figure 12: supernova and extreme-supernova time delay quotient estimations from simulation B. The upper row shows the estimations from the flux ratio, the second row shows the time delay quotient estimations, the third row shows the combined estimations and the lowest row shows the combined estimations using a prior on Ω_M. The 68.3 % confidence interval is within the white area, the 95 % is within the white-grey area and the 99 % is within the grey-black area.

5.2.2 Simulation B -Summing χ^2 in H_0-Ω_M Space

In simulation B the summing χ^2 in H_0-Ω_M space gives the contour regions as Fig. (13), where the two figure columns shows how dominant the value of η becomes. In the left column $\eta = 2.0$ and in right column $\eta = 1.5$. When using $\delta_\theta = 0.01''$, $\delta_t = 2.0$ [days] and $\delta_\eta = 0.1$ in this simulation the uncertainty from $\left(\frac{\partial \Delta t}{\partial \eta}\,\delta_\eta\right)$ becomes about 100 times larger than σ_{obs}.

Figure (13) shows that the summing χ^2-estimations gives no information of Ω_M and only H_0 can be estimated. The estimated values of H_0 are

B	Probability	Source A	Source B	Sum of χ^2	$\Omega_{M-prior}$
H_0	68.3 %	69^{+12}_{-11}	70^{+11}_{-12}	70^{+8}_{-9}	70^{+8}_{-7}
	95 %	69^{+18}_{-17}	70^{+17}_{-19}	70^{+12}_{-14}	70^{+12}_{-12}
	99 %	69^{+23}_{-21}	70^{+21}_{-23}	70^{+15}_{-17}	70^{+15}_{-15}

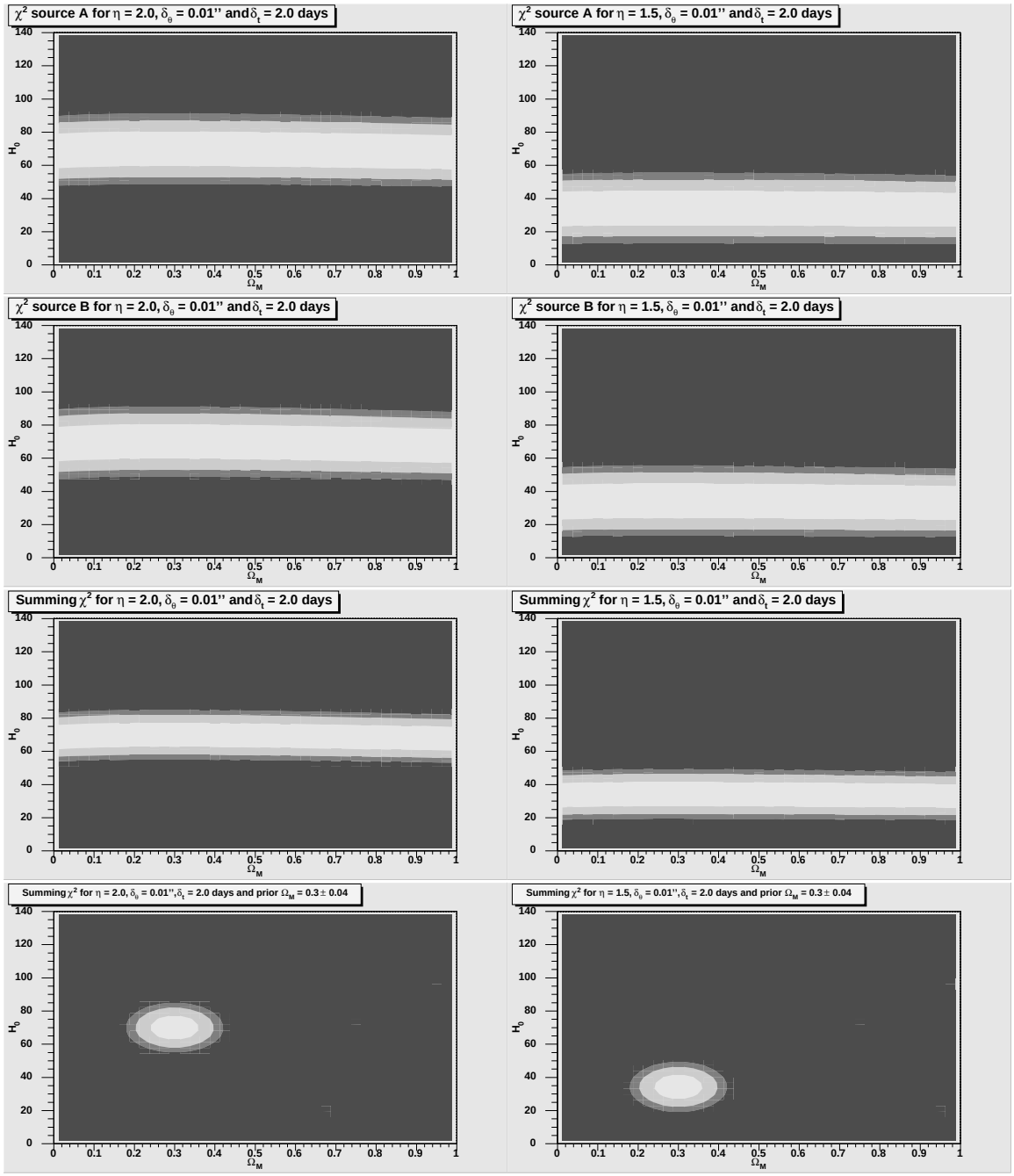

Figure 13: Summing χ^2 from simulation B. The left column shows estimations for $\eta = 2.0$ and the right shows estimations for $\eta = 1.5$, in both cases are$\delta_\theta = 0.01''$ and $\delta_t = 2.0$ [days]. From above, the first row shows estimations for source A alone, the second row shows estimations for source B alone, the third row shows estimations of the sum of χ^2 and the lowest row shows estimations of the sum of χ^2 with a $\Omega_{M-prior} = 0.30 \pm 0.04$. The 68.3 % confidence interval is within the white area, the 95 % is within the white-grey area and the 99 % is within the grey-black area.

5.3 Simulation C

In simulation C, a DOL-system is simulated with the observables

$$\begin{cases} z_l &= 0.85 \pm 0.001 \\ z_a &= 2.5 \pm 0.001 \\ z_b &= 3.0 \pm 0.001 \\ \sigma_v &= 375 \quad [\text{km s}^{-1}] \end{cases} \tag{105}$$

Using eq. (76) the image angles becomes

$$\begin{cases} \theta_{a_1} &= 3.01 \quad [\text{arcsec}] \\ \theta_{a_2} &= 1.03 \quad [\text{arcsec}] \\ \theta_{b_1} &= 3.26 \quad [\text{arcsec}] \\ \theta_{b_2} &= 1.12 \quad [\text{arcsec}] \end{cases} \Longrightarrow \begin{cases} \theta_{E_a} &= 2.02 \quad [\text{arcsec}] \\ \theta_{E_b} &= 2.19 \quad [\text{arcsec}] \end{cases} \tag{106}$$

Using these θ-values and $\Omega_M = 0.30 \pm 0.04$, the SIS time delay for each source (eq. (65)) and the quotient between them becomes

$$\begin{cases} \Delta t_a &= 658 \quad [\text{days}] \\ \Delta t_b &= 713 \quad [\text{days}] \end{cases} \Longrightarrow q_{sim} = \begin{cases} 0.923 \pm 0.004 & , \text{quasar} \\ 0.923 \pm 0.003 & , \text{nova-quasar} \\ 0.923 \pm 0.0003 & , \text{supernova} \end{cases} \tag{107}$$

5.3.1 Simulation C - Time Delay Quotient

Like simulation B, simulation C only gives useful time delay quotients- and flux ratios estimations in the extreme-supernova sub-simulation. Therefore, from simulation C no plots are shown from the quasar- and the nova-quasar sub-simulations, the estimated contour regions from the other two sub-simulations are shown in Fig. (14). Simulation C gives the following values for Ω_M and η

Estimation	Probability	Ω_M	η	σ_{th}
Flux	68.3 %	—	$2.00^{+0.35}_{-0.52}$	—
	95 %	—	$2.00^{+0.53}_{-1.05}$	
	99 %	—	$2.00^{+0.64}$	
quasar	68.3 %	—	$2.00^{+0.35}_{-0.52}$	$\sigma_{th} = 6\,\sigma_{obs}$
	95 %	—	$2.00^{+0.53}_{-1.05}$	
	99 %	—	$2.00^{+0.64}$	
nova-quasar	68.3 %	—	$2.00^{+0.35}_{-0.52}$	$\sigma_{th} = 10\,\sigma_{obs}$
	95 %	—	$2.00^{+0.53}_{-1.05}$	
	99 %	—	$2.00^{+0.64}$	
super-nova	68.3 %	—	$2.00^{+0.35}_{-0.52}$	$\sigma_{th} = 1000\,\sigma_{obs}$
	95 %	—	$2.00^{+0.53}_{-1.05}$	
	99 %	—	$2.00^{+0.64}$	
extreme super-nova	68.3 %	$0.30^{+0.24}_{-0.16}$	$2.00^{+0.35}_{-0.52}$	$\sigma_{th} = 200\,\sigma_{obs}$
	95 %	$0.30^{+0.47}$	$2.00^{+0.53}_{-1.05}$	
	99 %	$0.30^{+0.65}$	$2.00^{+0.64}$	

Due to the degeneracy that appears from the extreme-supernova time delay quotient estimation, the Ω_M value for 68.3 % corresponds to the right confidence region in fig. (14).

5.3.2 Simulation C -Summing χ^2 in H_0-Ω_M Space

In simulation C the summing χ^2 in H_0-Ω_M space gives the contour regions as Fig. (15), where the two figure columns shows how dominant the value of η becomes. In the left column $\eta = 2.0$ and in right column $\eta = 1.5$. When using $\delta_\theta = 0.01''$, $\delta_t = 2.0$ [days] and $\delta_\eta = 0.1$ in this simulation the uncertainty from $\left(\frac{\partial \Delta t}{\partial \eta}\,\delta_\eta\right)$ becomes about 100 times larger than σ_{obs}.

Figure (15) shows that the summing χ^2-estimations gives no information of Ω_M and only H_0 can be estimated. The estimated values of H_0 are

C	Probability	Source A	Source B	Sum of χ^2	$\Omega_{M-prior}$
H_0	68.3 %	66^{+16}_{-12}	64^{+18}_{-11}	70^{+8}_{-14}	70^{+8}_{-7}
	95 %	66^{+22}_{-18}	64^{+24}_{-17}	70^{+16}_{-21}	70^{+12}_{-12}
	99 %	66^{+26}_{-22}	64^{+29}_{-20}	70^{+16}_{-21}	70^{+15}_{-15}

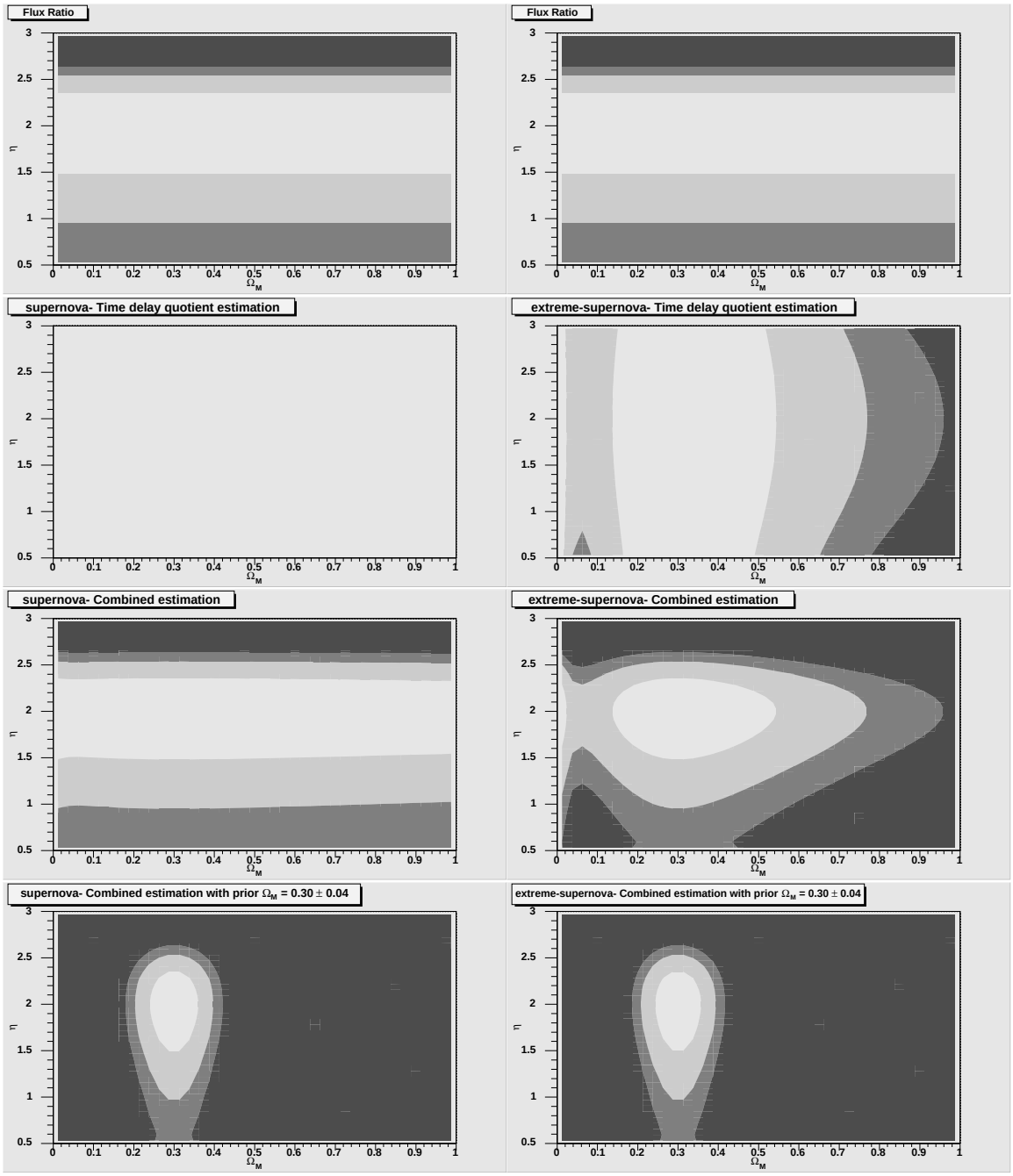

Figure 14: supernova and extreme-supernova time delay quotient estimations from simulation C. The upper row shows the estimations from the flux ratio, the second row shows the time delay quotient estimations, the third row shows the combined estimations and the lowest row shows the combined estimations using a prior on Ω_M. The 68.3 % confidence interval is within the white area, the 95 % is within the white-grey area and the 99 % is within the grey-black area.

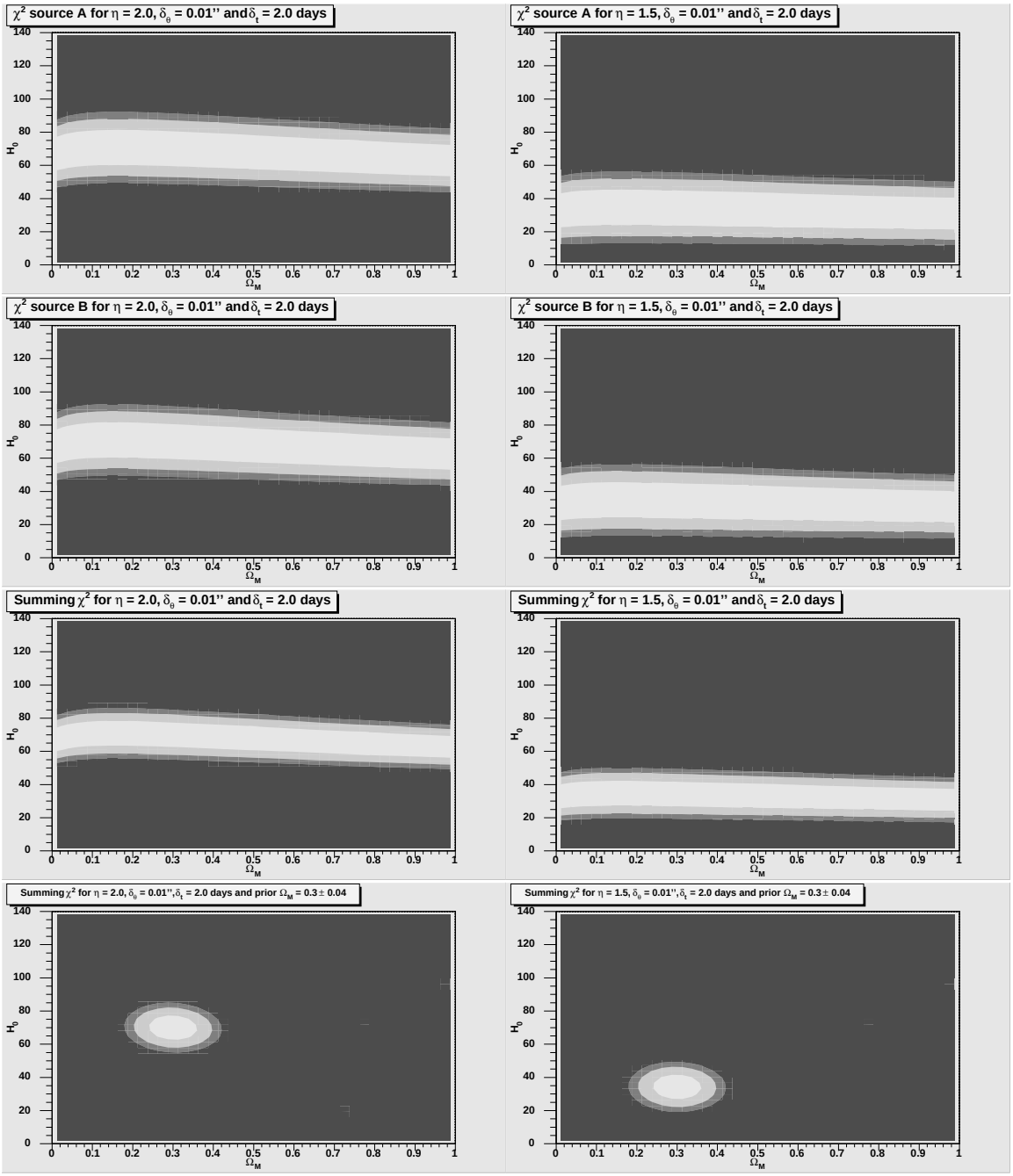

Figure 15: Summing χ^2 from simulation C. The left column shows estimations for $\eta = 2.0$ and the right shows estimations for $\eta = 1.5$, in both cases are $\delta_\theta = 0.01''$ and $\delta_t = 2.0$ [days]. From above, the first row shows estimations for source A alone, the second row shows estimations for source B alone, the third row shows estimations of the sum of χ^2 and the lowest row shows estimations of the sum of χ^2 with a $\Omega_{M-prior} = 0.30 \pm 0.04$. The 68.3 % confidence interval is within the white area, the 95 % is within the white-grey area and the 99 % is within the grey-black area.

5.4 Simulation D

In simulation D, a DOL-system is simulated with the observables

$$\begin{cases} z_l &= 0.4 \pm 0.001 \\ z_a &= 0.75 \pm 0.001 \\ z_b &= 3.0 \pm 0.001 \\ \sigma_v &= 375 \quad [\text{km s}^{-1}] \end{cases} \tag{108}$$

Using eq. (76) the image angles becomes

$$\begin{cases} \theta_{a_1} &= 2.50 \quad [\text{arcsec}] \\ \theta_{a_2} &= 0.86 \quad [\text{arcsec}] \\ \theta_{b_1} &= 4.57 \quad [\text{arcsec}] \\ \theta_{b_2} &= 1.56 \quad [\text{arcsec}] \end{cases} \Longrightarrow \begin{cases} \theta_{E_a} &= 1.68 \quad [\text{arcsec}] \\ \theta_{E_b} &= 3.07 \quad [\text{arcsec}] \end{cases} \tag{109}$$

Using these θ-values and $\Omega_M = 0.30 \pm 0.04$, the SIS time delay for each source (eq. (65)) and the quotient between them becomes

$$\begin{cases} \Delta t_a &= 290 \quad [\text{days}] \\ \Delta t_b &= 529 \quad [\text{days}] \end{cases} \Longrightarrow q_{sim} = \begin{cases} 0.548 \pm 0.004 & \text{, quasar} \\ 0.548 \pm 0.002 & \text{, nova-quasar} \\ 0.548 \pm 0.0003 & \text{, supernova} \end{cases} \tag{110}$$

5.4.1 Simulation D - Time Delay Quotient

In simulation D the χ^2-tests from the time delay quotients and the flux ratios gives the contour regions as Fig. (16) and (17), which gives the following values for Ω_M and η

Estimation	Probability	Ω_M	η	σ_{th}
Flux	68.3 %	—	$2.00^{+0.35}_{-0.52}$	—
	95 %	—	$2.00^{+0.53}_{-1.05}$	
	99 %	—	$2.00^{+0.64}$	
quasar	68.3 %	$0.30^{+0.38}$	$2.00^{+0.35}_{-0.52}$	$\sigma_{th} = 2\,\sigma_{obs}$
	95 %	$0.30^{+0.66}$	$2.00^{+0.53}_{-1.05}$	
	99 %	—	$2.00^{+0.64}$	
nova-quasar	68.3 %	$0.30^{+0.31}$	$2.00^{+0.35}_{-0.52}$	$\sigma_{th} = 9\,\sigma_{obs}$
	95 %	$0.30^{+0.55}$	$2.00^{+0.53}_{-1.05}$	
	99 %	—	$2.00^{+0.64}$	
super-nova	68.3 %	$0.30^{+0.30}$	$2.00^{+0.35}_{-0.52}$	$\sigma_{th} = 300\,\sigma_{obs}$
	95 %	$0.30^{+0.52}$	$2.00^{+0.53}_{-1.05}$	
	99 %	$0.30^{+0.68}$	$2.00^{+0.64}$	
extreme super-nova	68.3 %	$0.30^{+0.06}_{-0.06}$	$2.00^{+0.35}_{-0.52}$	$\sigma_{th} = 10\,\sigma_{obs}$
	95 %	$0.30^{+0.10}_{-0.11}$	$2.00^{+0.53}_{-1.05}$	
	99 %	$0.30^{+0.12}_{-0.28}$	$2.00^{+0.64}$	

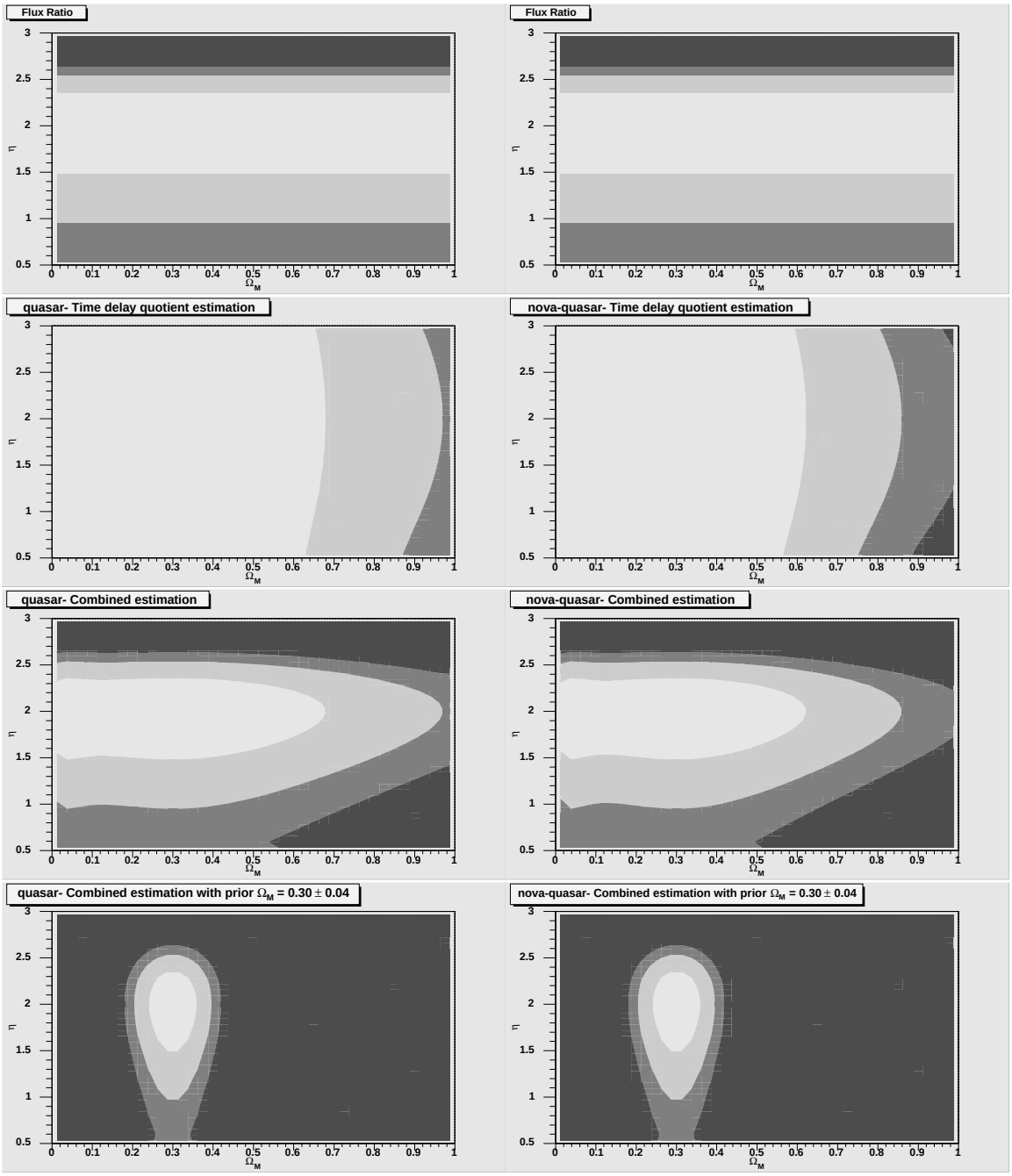

Figure 16: quasar and nova-quasar time delay quotient estimations from simulation D. The upper row shows the estimations from the flux ratio, the second row shows the time delay quotient estimations, the third row shows the combined estimations and the lowest row shows the combined estimations using a prior on Ω_M. The 68.3 % confidence interval is within the white area, the 95 % is within the white-grey area and the 99 % is within the grey-black area.

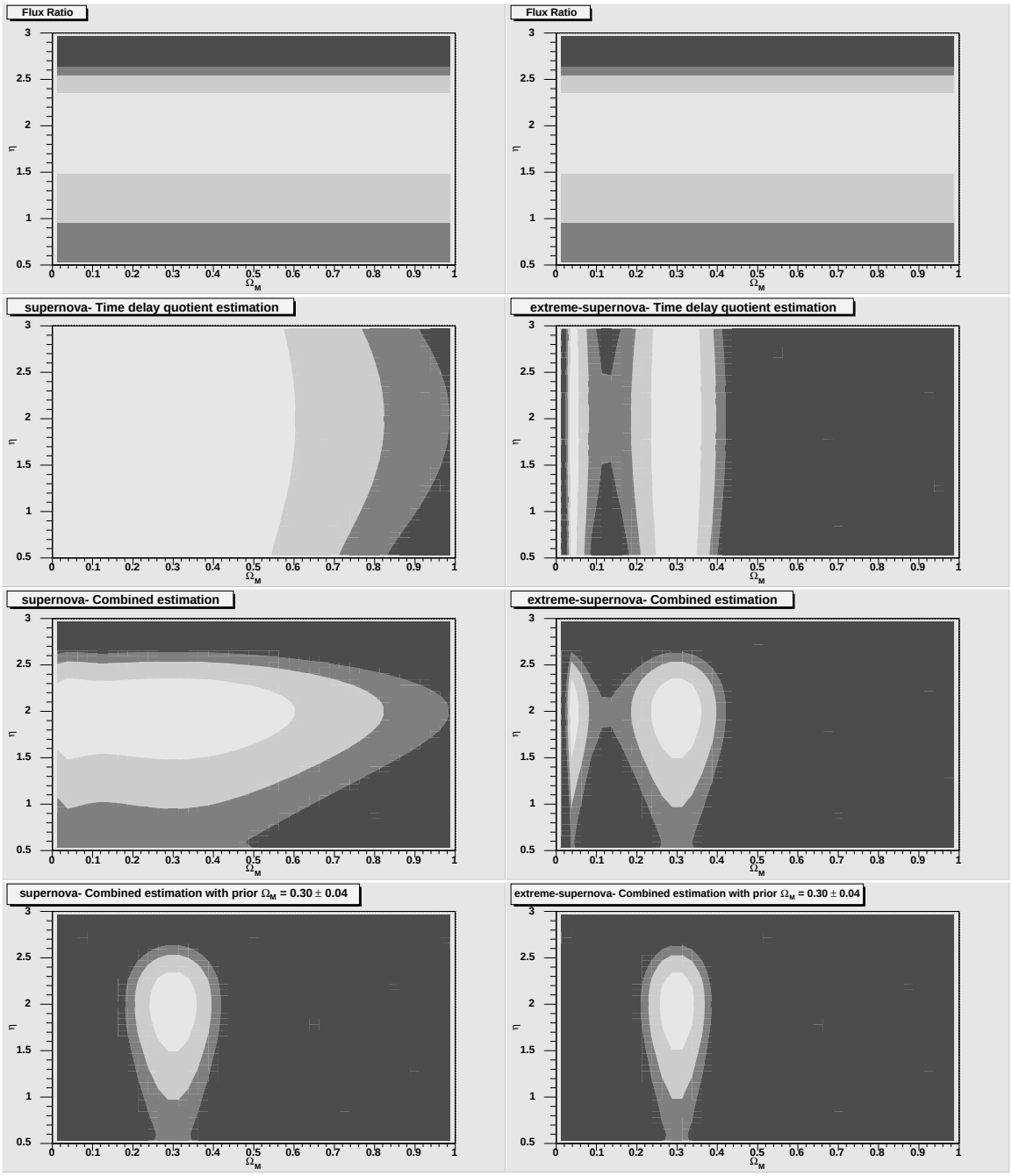

Figure 17: supernova and extreme-supernova time delay quotient estimations from simulation D. The upper row shows the estimations from the flux ratio, the second row shows the time delay quotient estimations, the third row shows the combined estimations and the lowest row shows the combined estimations using a prior on Ω_M. The 68.3 % confidence interval is within the white area, the 95 % is within the white-grey area and the 99 % is within the grey-black area.

Due to the degeneracy that appears in the extreme-supernova time delay quotient estimation, the Ω_M values for 68.3 % and 95 % corresponds to the right confidence region in fig. (17).

5.4.2 Simulation D -Summing χ^2 in H_0-Ω_M Space

In simulation D the summing χ^2 in H_0-Ω_M space gives the contour regions as Fig. (18), where the two figure columns shows how dominant the value of η becomes. In the left column $\eta = 2.0$ and in right column $\eta = 1.5$. When using $\delta_\theta = 0.01''$, $\delta_t = 2.0$ [days] and $\delta_\eta = 0.1$ in this simulation the uncertainty from $\left(\frac{\partial \Delta t}{\partial \eta}\,\delta_\eta\right)$ becomes about 100 times larger than σ_{obs}.

Figure (18) shows that the summing χ^2-estimations gives no information of Ω_M and only H_0 can be estimated. The estimated values of H_0 are

D	Probability	Source A	Source B	Sum of χ^2	$\Omega_{M-prior}$
H_0	68.3 %	69^{+12}_{-11}	69^{+12}_{-13}	69^{+9}_{-9}	70^{+8}_{-7}
	95 %	69^{+18}_{-17}	69^{+18}_{-19}	69^{+13}_{-14}	70^{+12}_{-12}
	99 %	69^{+23}_{-21}	69^{+23}_{-23}	69^{+16}_{-16}	70^{+15}_{-15}

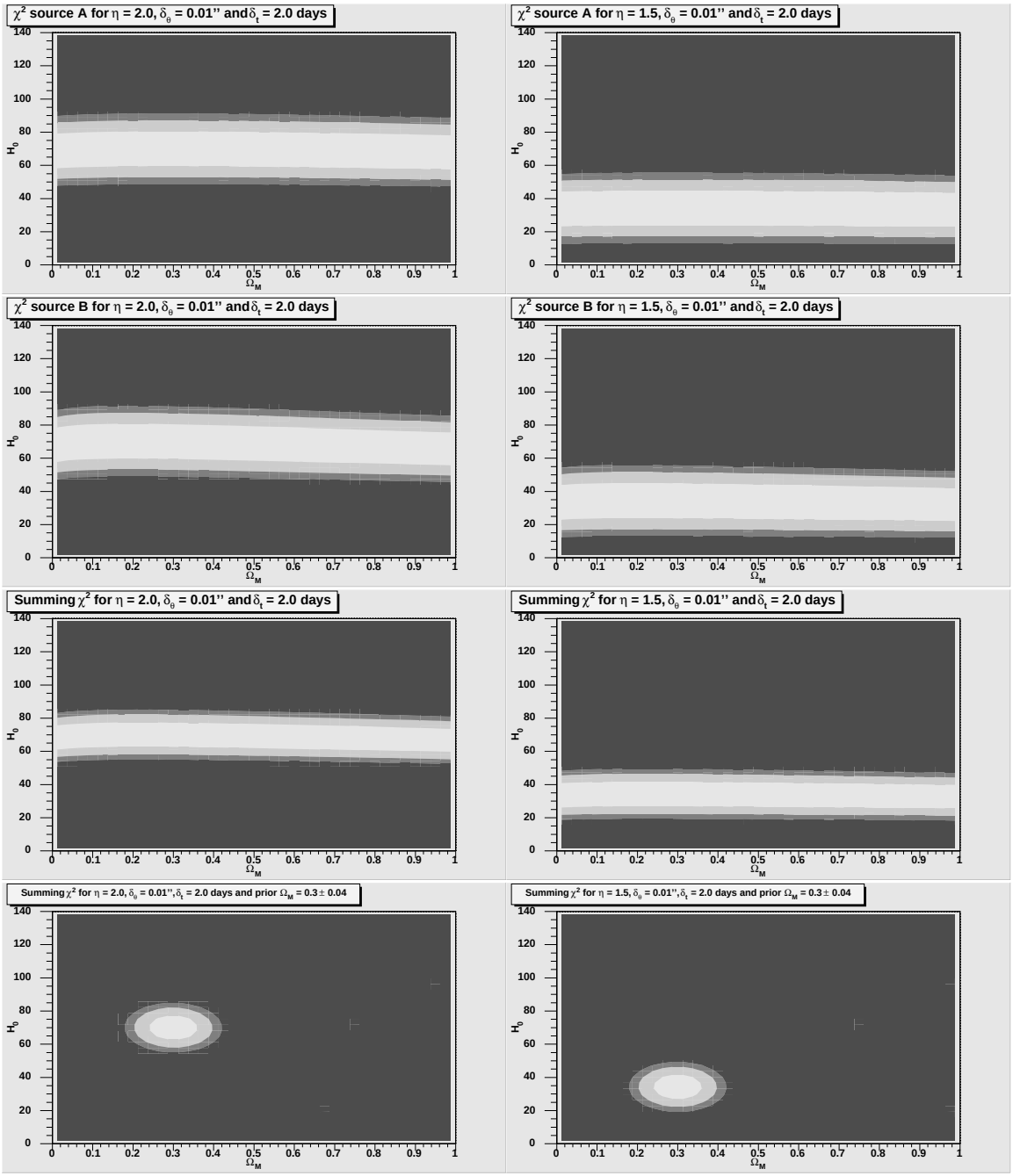

Figure 18: Summing χ^2 from simulation D. The left column shows estimations for $\eta = 2.0$ and the right shows estimations for $\eta = 1.5$, in both cases are $\delta_\theta = 0.01''$ and $\delta_t = 2.0$ [days]. From above, the first row shows estimations for source A alone, the second row shows estimations for source B alone, the third row shows estimations of the sum of χ^2 and the lowest row shows estimations of the sum of χ^2 with a $\Omega_{M-prior} = 0.30 \pm 0.04$. The 68.3 % confidence interval is within the white area, the 95 % is within the white-grey area and the 99 % is within the grey-black area.

5.5 Simulation E

In simulation E, a DOL-system is simulated with the observables

$$\begin{cases} z_l &= 0.4 \pm 0.001 \\ z_a &= 0.75 \pm 0.001 \\ z_b &= 3.0 \pm 0.001 \\ \sigma_v &= 475 \quad [\text{km s}^{-1}] \end{cases} \tag{111}$$

Using eq. (76) the image angles becomes

$$\begin{cases} \theta_{a_1} &= 4.02 \quad [\text{arcsec}] \\ \theta_{a_2} &= 1.37 \quad [\text{arcsec}] \\ \theta_{b_1} &= 7.33 \quad [\text{arcsec}] \\ \theta_{b_2} &= 2.51 \quad [\text{arcsec}] \end{cases} \Longrightarrow \begin{cases} \theta_{E_a} &= 2.70 \quad [\text{arcsec}] \\ \theta_{E_b} &= 4.92 \quad [\text{arcsec}] \end{cases} \tag{112}$$

Using these θ-values and $\Omega_M = 0.30 \pm 0.04$, the SIS time delay for each source (eq. (65)) and the quotient between them becomes

$$\begin{cases} \Delta t_a &= 747 \quad [\text{days}] \\ \Delta t_b &= 1363 \quad [\text{days}] \end{cases} \Longrightarrow q_{sim} = \begin{cases} 0.548 \pm 0.002 & \text{, quasar} \\ 0.548 \pm 0.0008 & \text{, nova-quasar} \\ 0.548 \pm 0.0001 & \text{, supernova} \end{cases} \tag{113}$$

5.5.1 Simulation E - Time Delay Quotient

In simulation E the χ^2-tests from the time delay quotients and the flux ratios gives the contour regions as Fig. (19) and (20), which gives the following values for Ω_M and η

Estimation	Probability	Ω_M	η	σ_{th}
Flux	68.3 %	—	$2.00^{+0.35}_{-0.52}$	—
	95 %	—	$2.00^{+0.53}_{-1.05}$	
	99 %	—	$2.00^{+0.64}$	
quasar	68.3 %	$0.30^{+0.20}$	$2.00^{+0.35}_{-0.52}$	$\sigma_{th} = 4\,\sigma_{obs}$
	95 %	$0.30^{+0.33}$	$2.00^{+0.53}_{-1.05}$	
	99 %	$0.30^{+0.42}$	$2.00^{+0.64}$	
nova-quasar	68.3 %	$0.30^{+0.19}$	$2.00^{+0.35}_{-0.52}$	$\sigma_{th} = 20\,\sigma_{obs}$
	95 %	$0.30^{+0.31}$	$2.00^{+0.53}_{-1.05}$	
	99 %	$0.30^{+0.39}$	$2.00^{+0.64}$	
super-nova	68.3 %	$0.30^{+0.18}$	$2.00^{+0.35}_{-0.52}$	$\sigma_{th} = 1000\,\sigma_{obs}$
	95 %	$0.30^{+0.30}$	$2.00^{+0.53}_{-1.05}$	
	99 %	$0.30^{+0.38}$	$2.00^{+0.64}$	
extreme super-nova	68.3 %	$0.30^{+0.04}_{-0.04}$	$2.00^{+0.35}_{-0.52}$	$\sigma_{th} = 30\,\sigma_{obs}$
	95 %	$0.30^{+0.06}_{-0.06}$	$2.00^{+0.53}_{-1.05}$	
	99 %	$0.30^{+0.07}_{-0.08}$	$2.00^{+0.64}$	

Due to the degeneracy that appears in the extreme-supernova time delay quotient estimation, the Ω_M values corresponds to the right confidence region in fig. (19).

5.5.2 Simulation E -Summing χ^2 in H_0-Ω_M Space

In simulation E the summing χ^2 in H_0-Ω_M space gives the contour regions as Fig. (21), where the two figure columns shows how dominant the value of η becomes. In the left column $\eta = 2.0$ and in right column $\eta = 1.5$. When using $\delta_\theta = 0.01''$, $\delta_t = 2.0$ [days] and $\delta_\eta = 0.1$ in this simulation the uncertainty from $\left(\frac{\partial \Delta t}{\partial \eta}\,\delta_\eta\right)$ becomes about 100-1000 times larger than σ_{obs}.

Figure (21) shows that the summing χ^2-estimations gives no information of Ω_M and only H_0 can be estimated. The estimated values of H_0 are

E	Probability	Source A	Source B	Sum of χ^2	$\Omega_{M-prior}$
H_0	68.3 %	69^{+12}_{-11}	69^{+12}_{-13}	69^{+9}_{-9}	70^{+8}_{-7}
	95 %	69^{+18}_{-18}	69^{+18}_{-19}	69^{+13}_{-14}	70^{+12}_{-12}
	99 %	69^{+23}_{-21}	69^{+23}_{-23}	69^{+17}_{-16}	70^{+15}_{-15}

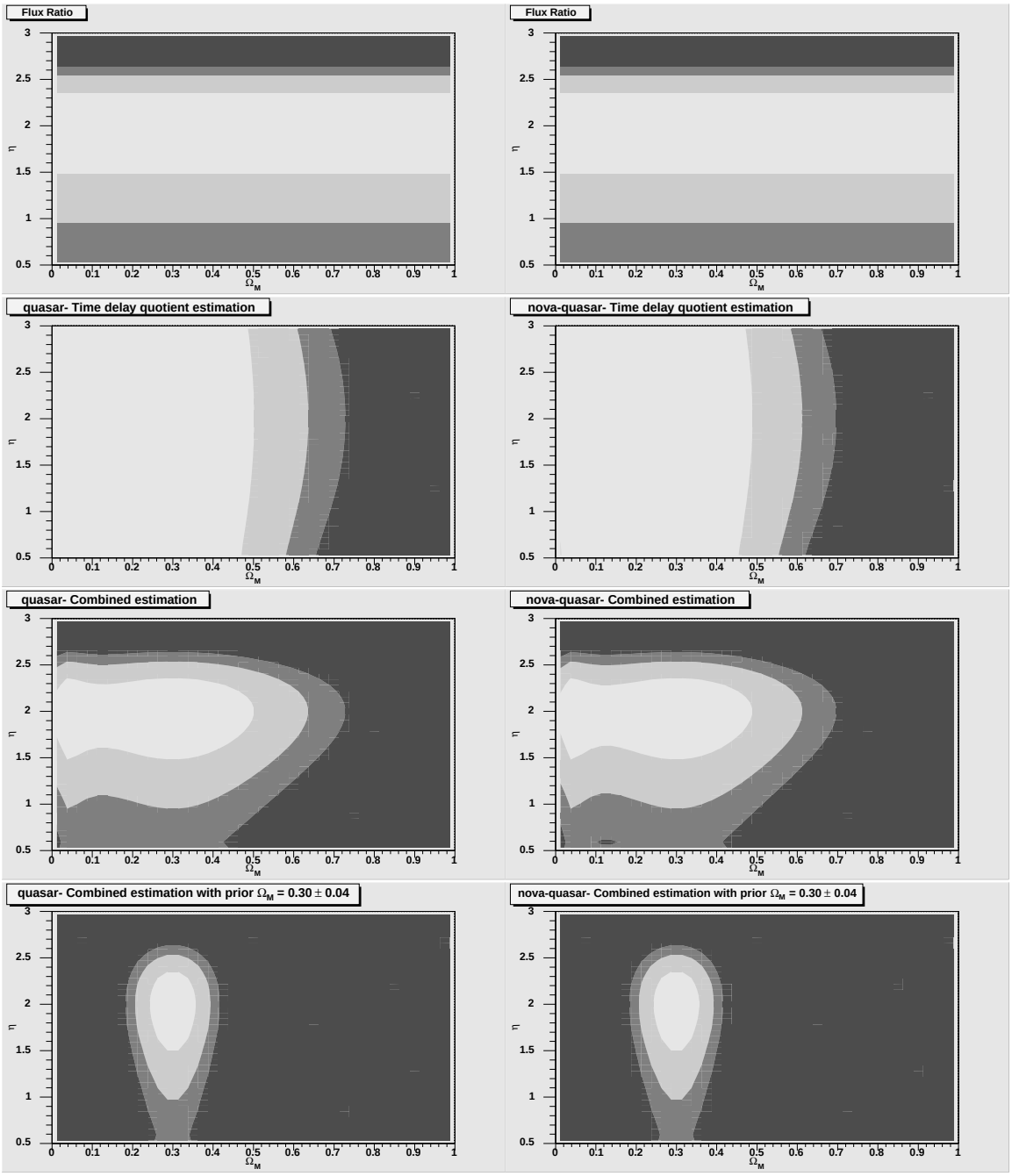

Figure 19: quasar and nova-quasar time delay quotient estimations from simulation E. The upper row shows the estimations from the flux ratio, the second row shows the time delay quotient estimations, the third row shows the combined estimations and the lowest row shows the combined estimations using a prior on Ω_M. The 68.3 % confidence interval is within the white area, the 95 % is within the white-grey area and the 99 % is within the grey-black area.

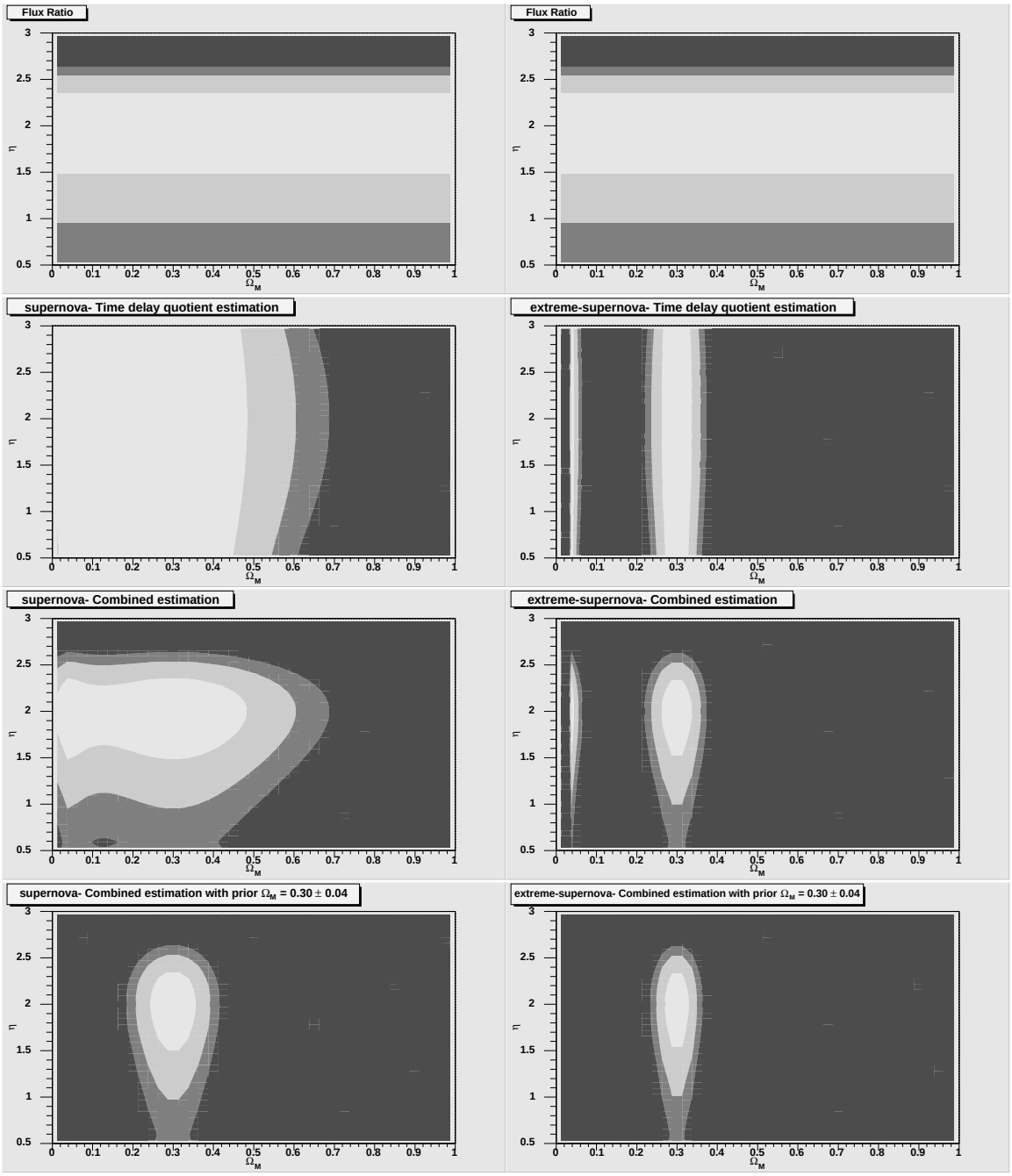

Figure 20: supernova and extreme-supernova time delay quotient estimations from simulation E. The upper row shows the estimations from the flux ratio, the second row shows the time delay quotient estimations, the third row shows the combined estimations and the lowest row shows the combined estimations using a prior on Ω_M. The 68.3 % confidence interval is within the white area, the 95 % is within the white-grey area and the 99 % is within the grey-black area.

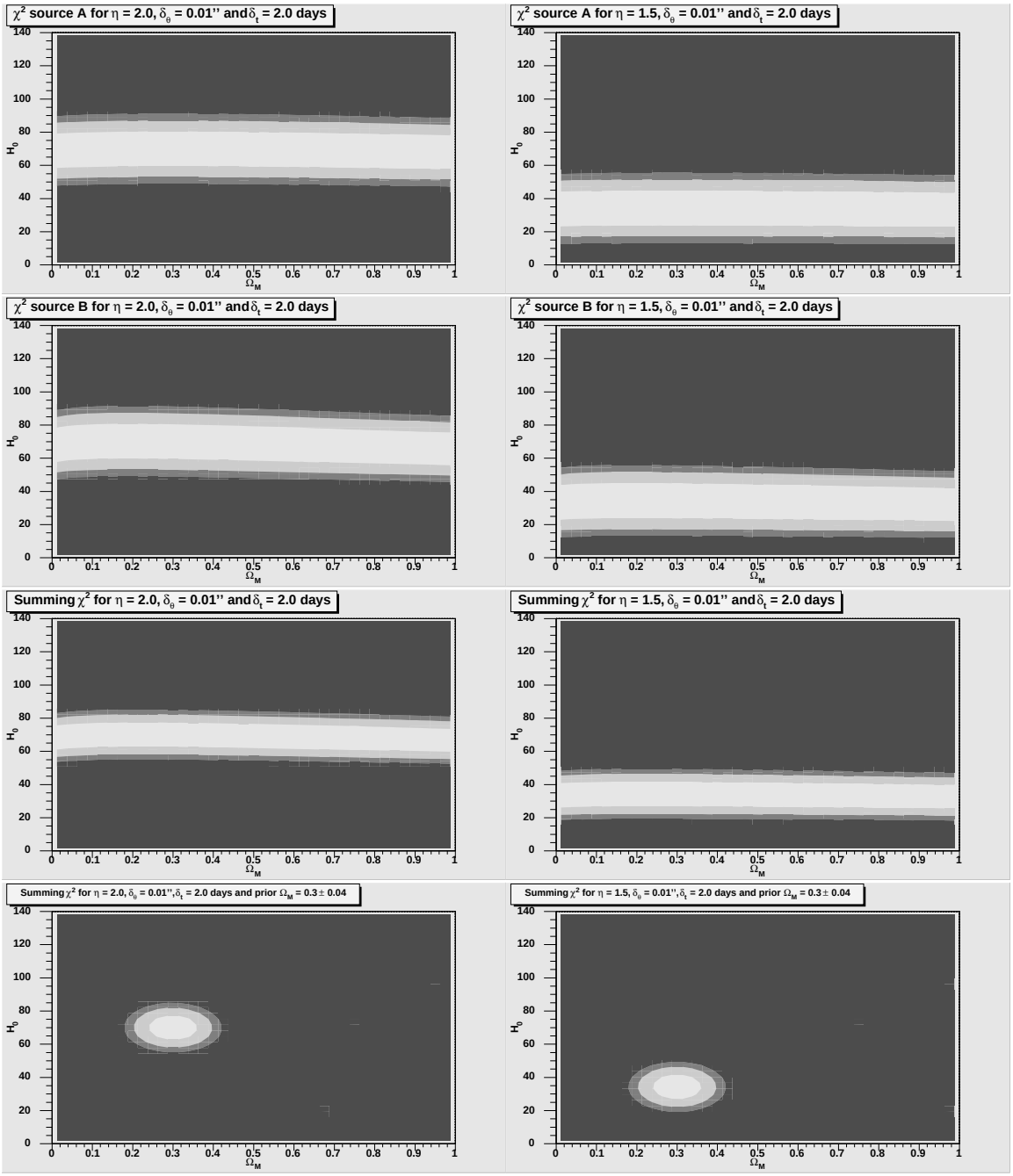

Figure 21: Summing χ^2 from simulation E. The left column shows estimations for $\eta = 2.0$ and the right shows estimations for $\eta = 1.5$, in both cases are $\delta_\theta = 0.01''$ and $\delta_t = 2.0$ [days]. From above, the first row shows estimations for source A alone, the second row shows estimations for source B alone, the third row shows estimations of the sum of χ^2 and the lowest row shows estimations of the sum of χ^2 with a $\Omega_{M-prior} = 0.30 \pm 0.04$. The 68.3 % confidence interval is within the white area, the 95 % is within the white-grey area and the 99 % is within the grey-black area.

6 Discussion

This discussion part is split into four sections where the first section discusses the quotient estimations, the second discusses the summing χ^2 estimations, the third discusses how the estimations can be improved and the fourth gives a summary.

6.1 Quotient Estimations

Since the proportions between the image angles are the same, the estimated flux ratio becomes the same in all simulations, and since the time delay quotient estimations does not give any information of η, the flux ratio estimation estimates η alone. Even when using smaller δ_t and δ_θ and a prior on Ω_M, the combined estimation does not improve the flux ratio estimation, and as the image angles $\frac{\theta_1}{\theta_2} \to 1$ the estimation of η becomes worse, eq. (84).

Thus, the estimation of η depends on the observed uncertainty in the flux ratio and on the fraction between the image angles, and larger angle differences improves the estimation.

When simulating my DOL-systems, four factors becomes important for the estimations of Ω_M; the separation between the sources, the image separations, the velocity dispersion in the lens and the uncertainty in the image angles.

That larger separations between the sources gives better estimations can be seen when comparing a simulation with sources close to each other with a simulation where the sources are more separated, e.g. simulation B and D. The important factor here is the *angular separation ratio* $\frac{D_a D_{lb}}{D_b D_{la}}$ which increases with increasing angular separations, when b is the most distant source. Hence, with increasing angular separation ratio the contour regions narrows.

Thus, due to larger source separations better estimations are given in simulation D than in B, where as in simulation C useful results are given first when using $\delta_{\theta_i} = 0.002''$ and $\delta_t = 0.15$ [days].

Relative to simulation B the sources in C are at higher redshifts, and since z_l and D_l are larger the time delays becomes larger. Regardless of the high redshifts in simulation C the image angles from source b becomes almost the same as in B, which means that the factors $\frac{D_{lb}}{D_b}$ in eq. (62) are almost the same. This is due to the fact that the angular distance decreases after a certain redshift. For instance, the angular distance to source b is greater in simulation B than in C.

Since the image angles are proportional to $\frac{D_{ls}}{D_s}$, eqs. (62) and (63), the image separation for source a becomes larger in C, which then increases the time delay quotient, eq. (85). Thus, due to larger image separations the estimations becomes better in simulation C than in B.

The different results from the simulations D and E also confirms that

larger image separations improves the estimation. The value for σ_v is the only difference in these simulations and according to eq. (62) higher σ_v gives larger image separations, which then increases the time delay quotient.

When simulating with smaller uncertainties in the observed time delays, the estimation of Ω_M improves very little compared with the improvements that smaller image angle uncertainties gives. Even when using the small uncertainties in the extreme-supernova sub-simulations, all estimations are dominated by the image angle uncertainty. For instance in simulation D, the differences in Ω_M's confidence intervals from the sub-simulations with $\delta_{\theta_i} = 0.01''$ are very small compared with the difference when using $\delta_{\theta_i} = 0.002''$ from the extreme-supernova sub-simulation. Also, the farther the lens is the more the uncertainty from the image angle dominates the estimations, e.g. the domination is bigger in simulation A and C than in B and D where in all simulations the velocity dispersions are the same.

Therefore, the observed uncertainties used in the sub-simulations shows that the estimations of Ω_M are sensitive to errors from the image angle measurements.

Thus, to obtain a good estimation of Ω_M by using time delays from gravitational lensing with multiple sources one has to find a system with supernovae at very different angular distances, which have accurately measured image angles that are significantly separated by a not so far away lens.

6.2 Summing χ^2 Estimations

No matter how large object- and image separations one simulates, the improvement in the parameter estimations from summing χ^2 is marginal. All my simulated DOL-systems gives that H_0 can be estimated while Ω_M can not and that the error in η dominates the total error. Even when simulating systems with source separations of a few redshifts, the contour curves have the same band-shape.

Equation (70) shows that the power law time delay is proportional to η as

$$\Delta t \propto (\eta - 1)\left(1 - (2 - \eta)^2 \dots\right) \tag{114}$$

so changing η with 25 % from $\eta = 2.0$ to $\eta = 1.5$, makes a change in Δt about 42 %. When simulating DOL-systems with $\eta = 1.5$ the estimated value for H_0 becomes 42-53 % lower than in a system with $\eta = 2.0$. Therefore, the result depends on the value chosen for η.

In all simulations, when summing the χ^2 from both sources the estimation of H_0 improves around 25 % compared with the χ^2 estimations from each object alone.

The simulations also shows that the farther the lens is the worser the estimations of H_0 becomes, independent of the lens mass and object- and

image separations. For instance, due to the higher lens redshift in simulation A and C the estimation of H_0 becomes worse than in the other simulations.

Thus, to obtain a good estimation of H_0 by using time delays from gravitational lensing with multiple sources one has to find a system with sources lensed by a not so far away lens. With better knowledge of the lens properties and by summing each sources χ^2-tested time delays, the estimation of H_0 improves.

6.3 Improvements

I believe the future of using time delays from a DOL-system to investigate the values of η, Ω_M and H_0 depends on improvements in many fields.

First, of course, a DOL-system with measurable time delays has to be found. The Cosmic Lens All-Sky Survey (CLASS), an international program to create the largest and best studied statistical sample of radio-loud gravitationally lensed systems, has observed 13783 radio sources where 16 were found to be gravitational lensed system with multiple images [16], which gives a probability of 10^{-3} to find a gravitational lensed system in every survey. Thus, the probability to find a radio source DOL-system becomes 10^{-6}.

According to Goobar *et al.* 2002 [11], with the future instruments as the SNAP and NGST satellites it will become possible to observe several hundred lensed core-collapse supernovae with multiple images. Therefore, it may be possible to observe DOL-systems with well measurable time delays in these future surveys.

When estimating Ω_M by using supernova time delays, it can be difficult to get small uncertainties in the image angles and not too long time delays. For instance, from the observed four multiple images system Abell 2218, Soucail, Kneib and Golse (2004) [26] reports a velocity dispersion of $\sigma_v \approx 1370$ [km s^{-1}] which means that if Abell 2218 had been lensing supernovae the measured time delays may have been too long, see Fig. (7). Time delays about several years may be hard or impossible to measure.

Another important factor when estimating Ω_M with time delay quotients is the angular separation between the objects. For instance, the more distant the lens, the longer time delays, which the time delays from the same source b in the simulations C and D shows. Therefore, to estimate Ω_M the satellite observations mentioned above has to find well angular separated supernovae lensed by a not too distant and massive object.

Since the summing χ^2 estimation is so dependent on η and not on the angular separation between the objects, the summing χ^2 estimation could be extended to sum χ^2 from several lensed supernovae and thereby improve the estimation of H_0. However, the probability that the satellite observations finds several supernovae lensed by the same lens is very small. From the CLASS survey one finds that the probability to find three sources lensed by

the same lens is 10^{-9} and for four sources the probability becomes 10^{-12}, etc.

6.4 Summary

Time delays and flux ratios from gravitational lensing with multiple sources can be used to estimate the logarithmic slope of the density parameter η, the matter energy density parameter Ω_M and the Hubble constant H_0. However, each parameter estimation requires different properties of the gravitationally lensed system.

η can be estimated by using the flux ratios, and improves with larger differences between the image angles and with smaller uncertainty in the observed flux ratio.

Ω_M can be estimated by using the quotient between the time delays, the estimation improves with larger sources- and image angle separations and with smaller uncertainties in the image angles and in the time delays.

H_0 can be estimated by combining the results from the individual time delays, this estimation improves with better knowledge of the lens properties, i.e. η, and when using a lens that is not too far away.

Acknowledgments

It is a pleasure to thank Edvard Mörtsell for supervising me through gravitational lensing and in the science of Cosmology, for all support and for always being there when I got stuck in papers and equations.

I would also like to thank Ulla Engberg, the student administrator at the Astronomy department.

Matthias Maercker, thank you for being such a cool classmate and for all funny and silly mischiefs we have done when we got tired of books and equations, like when we investigated Compton scattering in an excess of swivel chairs.

Tobbe, thanks for your interest in this thesis, for all comments and critics they really made sense, even though I have behaved as a stubborn "I can manage myself" little brother.

Emma Sjöström, thanks for all coffee breaks in the main library during the spring term.

Big Thanx to my rock'n'roll friends, grabbing some beers at a garage rock club with people who do not care about physics can sometimes be such a relief...

References

[1] Anderson, J., King, I R. *Toward High-Precision Astrometry with WFPC2.I. Deriving an Accurate Point-Spread Function*, Publications of the Astronomical Society of the Pacific, 112:1360-1382, October 2000.

[2] Bergström, L., Goobar, A. *Cosmology and Particlephysics*, Wiley, Chichester, 1999.

[3] Blandford, R., Narayan, R. *Fermat's Principle, Caustics, and the Classification of Gravitational Lens Images*, The Astrophysical Journal, 310:568-582, 15 Nov 1986.

[4] Cowan, G. *Statistical Data Analysis*, Clarendon Press, Oxford, 1998.

[5] Einstein, A. *Lens-like Action of a Star by the Deviation of Light in the Gravitational Field*, Science 84, 506, 1936.

[6] Feynman, R P. *QED- The Strange Theory of Light and Matter*, Penguin Books, London, England, 1990.

[7] Florentin-Nielsen, R. *Determination of Difference in Light Travel Time for QSO 0957 +561A, B*, Astronomy & Astrophysics, 138, L19-L20, 1984.

[8] Garavini G. *Type Ia Supernovae: Homogeneity and Diversity*, Department of Physics, Stockholm University, Sweden, 2004.

[9] Goliath, M., Amanullah, R., Astier, P., Goobar, A., Pain, R. *Supernovae and the Nature of the Dark Energy*, Astronomy & Astrophysics, 380, 6-18, 2001.

[10] Golse, G., Kneib, J P., Soucail, G. *Constraining the Cosmological Parameters Using Strong Lensing*, Astronomy & Astrophysics 387, 788-803, 2002.

[11] Goobar, A., Mörtsell, E., Amanullah, R., Nugent, P. *Cosmological Parameters from Lensed Supernovae*, Astronomy & Astrophysics, 393, 25-32, 2002.

[12] Kayser, R., Schramm, T., Nieser, L.(Eds). *Determining the Hubble Parameter- Sjur Refsdal*, Lecture Notes in Physics 406, Gravitational Lenses, Proceedings, Hamburg, Germany, 1991, Springer-Verlag, 1991.

[13] Kochanek, C S. *What Do Gravitational Lens Time Delay Measure?*, Astrophysical Journal, 578, 25, 2002.

[14] Kochanek, C S., Schechter, P L. *The Hubble Constant from Gravitational Lens Time Delays*, arXiv:astro-ph/0306040 v1,2 Jun 2003.

[15] Link, R., Pierce, M J. *Cosmological Parameters from Multiple-Arc Gravitational Lensing Systems*, Astrophysical Journal, 502:63:74, July 20 1998.

[16] Myers, S.T, *et al. The Cosmic Lens All-Sky Survey: I. Source selection and observation*, Monthly Notice of the Royal Astronomical Society, 341, 1, May 2003.

[17] Mörtsell, E., Dahle, H., Hannestad, S. *Probing Dark Matter Halos with Future Supernova Surveys*, arXiv:astro-ph/0406343 v1, 15 Jun 2004.

[18] Narayan, R., Bartelmann, M. *Lectures on Gravitational Lensing*, Proceedings of the 1995 Jerusalem Winter School: Edited by A, Dekel and J P, Ostriker, Cambridge University Press.

[19] Perkins, D. *Particle Astrophysics*, Oxford University Press, 2003.

[20] Raine, D J., Thomas, E G. *An Introduction to the Science of Cosmology*, Institute of Physics Publishing, Bristol and Philadelphia, 2001.

[21] Refsdal, S. *On the Possibility of Determining Hubble's Parameter and the Masses of Galaxies From the Gravitational Lens Effect*, Monthly Notice of the Royal Astronomical Society, 128, 307, 1964.

[22] Reiss, A G., *et al. Observational Evidence from Supernovae for an Accelerating Universe and a Cosmological Constant*, The Astronomical Journal, 1009-1038, Sept 1998.

[23] Schmidt, M. *A Star-Like Object With Large Red-Shift*, Nature, 197, 1040, 1963.

[24] Schneider, P. *Gravitational lensing as a probe of structure*, arXiv:astro-ph/0306465 v1,23 Jun 2003.

[25] Sharon, K., Broadhurst, T J., Benitez, N., Coe, D., Ford, H and ACS Science Team. *Strong Lensing Analysis of A1689 from Deep ACS Images*, arXiv:astro-ph/0409322 v1, 14 Sep 2004.

[26] Soucail, G., Kneib, J P., Golse, G. *Multiple-Images in the Cluster Lens Abell 2218: Constraining the Geometry of the Universe?*, arXiv:astro-ph/0402658 v1, 27 Feb 2004.

[27] Sparke, L S., Gallagher, S. *Galaxies in the Universe: An Introduction*, Cambridge University Press, 2000.

[28] Taylor, J R. *An Introduction to Error Analysis*, University Science Books, Sausalito, California, 1997.

[29] Tegmark, M., Strauss, M A., *et al. Cosmological Parameters from SDSS and WMAP*, arXiv:astro-ph/0310723 v2, 15 Jan 2004.

[30] Walsh, D., Carswell, R F., Weymann, R J. *0957+561 A,B: Twin Quasistellar Object Or Gravitational lens?*, Nature, 279, 381,1979.

[31] Witt H J., Mao, S., Keeton, C R. *Analytic Time Delays and H_0 Estimates for Gravitational Lenses*, Astrophysical Journal, 544:98-103, Nov 20 2000.

A The Geometric Time Delay

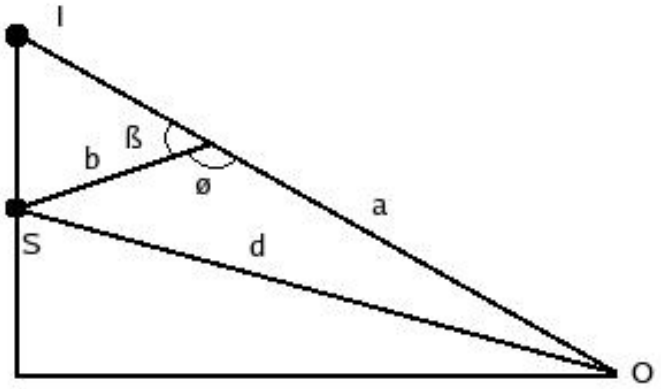

By geometry $\phi = \pi - \beta \Rightarrow \cos\phi = -\cos\beta$. Using the law of cosines gives

$$d^2 = a^2 + b^2 - 2\,ab\,\cos\phi = a^2 + b^2 + 2\,ab\,\cos\beta.$$

From the figure above, the time delay for a perturbed ray compared with an unperturbed ray is (c denotes the speed of the light)

$$c\cdot\Delta t = a+b-d = a+b-\sqrt{a^2+b^2+2\,ab\,\cos\beta} \approx \left[\cos\beta = 1-\frac{1}{2}\beta^2+\cdots\text{ (Taylor expansion)}\right] \approx$$

$$\approx \frac{ab}{2\,(a+b)}\,\beta^2 \approx \left[a+b\approx d\ (\beta\text{ is very small})\right] \approx \frac{ab}{2\,d}\,\beta^2.$$

Using eq. (5) the distances can be rewritten as

$$\left.\begin{array}{l} a = D_l\,(1+z_l) \\ b = D_{ls}\,(1+z_s) \\ d = D_s\,(1+z_s) \end{array}\right\} \Rightarrow\ c\cdot\Delta t = \frac{D_l D_{ls}}{2\,D_s}\,(1+z_l)\,\beta^2 = \left[\beta = \frac{D_s}{D_{ls}}\,(\theta_I-\theta_S)\right] =$$

$$= \frac{D_l D_s}{2\,D_{ls}}(1+z_l)\,(\theta_I-\theta_S)^2$$

where θ_I and θ_S are the angles between the image and optical axis respective the source and the optical axis and z_l and z_s are the redshifts to the lens respective to the source.

B SIS Surface-Mass Density

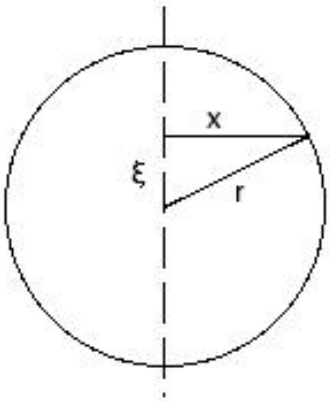

This figure shows a SIS lens with density $\rho(r)$. Using eq. (43) to integrate $\rho(r)$ for every mass sheet along x gives the surface-mass density in the lens plane as

$$\Sigma(\xi) = \int_{-\infty}^{0} \rho(r)\, dx + \int_{0}^{\infty} \rho(r)\, dx = 2 \int_{0}^{\infty} \rho(r)\, dx.$$

Equation (59) and the figure above gives

$$\left.\begin{array}{rcl} r^2 & = & x^2 + \xi^2 \\ \rho(r) & = & \frac{\sigma_v^2}{2\pi G} \frac{1}{r^2} \end{array}\right\} \Rightarrow \Sigma(\xi) = \frac{\sigma_v^2}{\pi G} \int_0^{\infty} \frac{dx}{x^2 + \xi^2} = \frac{\sigma_v^2}{\pi G} \frac{1}{\xi} \left[\arctan\left(\frac{x}{\xi}\right) \right]_0^{\infty} = \frac{\sigma_v^2}{2G} \frac{1}{\xi}.$$

C SIS Time Delay

The total time delay for an image is

$$\Delta t_i = \left[\frac{1+z_l}{c}\right]\left[\frac{D_l D_s}{D_{ls}}\right]\left[\frac{1}{2}(\theta_i-\beta)^2-\psi(\theta_i)\right]$$

where the lens potential $\psi(\theta_i)$ is related to the deflection angle α by eq. (64).

Consider now a SIS-lens which is producing two images at the angles θ_{a_1} respective θ_{a_2} from the lens center. According to the lens equation for a SIS-lens (eq. (63)) the images occurs at the radial distances

$$\theta_\pm = \mid \beta \mid \pm \alpha \implies \left\{ \begin{array}{lll} \theta_+ = & \theta_{a_1} & = \mid \beta \mid + \alpha \\ \theta_- = & -\theta_{a_2} & = \mid \beta \mid - \alpha \end{array} \right. \implies \alpha = \frac{\theta_{a_1}+\theta_{a_2}}{2}.$$

The time delay difference between the images is then

$$\Delta t_{A_2} - \Delta t_{A_1} = \left[\frac{1+z_l}{c}\right]\left[\frac{D_l D_s}{D_{ls}}\right]\left[\left[\frac{1}{2}(\theta_{a_2}-\beta)^2-\alpha\,\theta_{a_2}\right]-\left[\frac{1}{2}(\theta_{a_1}-\beta)^2-\alpha\,\theta_{a_1}\right]\right] =$$

$$= \left[\alpha = \frac{\theta_{a_1}+\theta_{a_2}}{2}\right] = \frac{1}{2}\left[\frac{1+z_l}{c}\right]\left[\frac{D_l D_s}{D_{ls}}\right](\theta_{a_1}^2-\theta_{a_2}^2) = \Delta t_{sis}.$$

D SIS Magnifications

Equation (49) gives the magnification for a circular symmetric lens as

$$\mu = \frac{\theta}{\beta}\frac{d\theta}{d\beta}.$$

Assume that $\beta > 0$ and a SIS-lens producing two images at θ_{a_1} and θ_{a_2}, appendix C show that the lens equation can be written as

$$\begin{aligned} \beta = \theta_{a_1} - \theta_E \quad &\Longrightarrow \quad d\beta = d\theta_{a_1}, \\ \beta = \theta_E - \theta_{a_2} \quad &\Longrightarrow \quad d\beta = -d\theta_{a_2}. \end{aligned}$$

The absolute magnitude for each image takes then the form

$$\mu_1 = \left| \frac{\theta_{a_1}}{\theta_{a_1} - \theta_E} \right|,$$

$$\mu_2 = \left| \frac{\theta_{a_2}}{\theta_E - \theta_{a_1}} \right|.$$

E Expressions for the Flux Ratios

In a power law lens the gravitational potential is given by

$$\psi(\theta_i) = \frac{\theta_E^2}{(3-\eta)} \left(\frac{\theta_i}{\theta_E} \right)^{3-\eta} = \frac{\theta_E^{\eta-1}}{(3-\eta)} \theta_i^{3-\eta}.$$

Equation (56) gives $\nabla_\theta \psi = \alpha$. Combining this with the expression for the gravitational potential and putting it into the lens equation gives

$$\beta = \theta - \alpha = \theta - \theta_i^{2-\eta}\, \theta_E^{\eta-1} \quad \Longrightarrow \quad d\beta = [\, 1 - (2-\eta)\, \theta_i^{1-\eta}\, \theta_E^{\eta-1}\,]\, d\theta_i.$$

By approximating that the gravitational potential of the lens affects the images in the same way, and that the condition $\beta < \alpha$ from eq. (63) holds, the lens equation gives for two images θ_1 and θ_2

$$\mid \beta \mid = \theta_1 - \theta_1^{2-\eta}\, \theta_E^{\eta-1} = -\theta_2 + \theta_2^{2-\eta}\, \theta_E^{\eta-1} \quad \Longleftrightarrow \quad \theta_E^{\eta-1} = \frac{\theta_1 + \theta_2}{\theta_1^{2-\eta} + \theta_2^{2-\eta}}.$$

Now, the magnification is given by

$$\mu = \left| \frac{\theta}{\beta} \frac{d\theta}{d\beta} \right|$$

and for one image from one source the magnification becomes

$$\mu = \left| \frac{\theta_i\, d\theta_i}{[\, 1 - (2-\eta)\, \theta_i^{1-\eta}\, \theta_E^{\eta-1}\,]\, d\theta_i} \right| = \left| \frac{\theta_i}{1 - (2-\eta)\, \theta_i^{1-\eta}\, \theta_E^{\eta-1}} \right|.$$

Since the flux ratio is the ratio between the magnifications, $r = \mu_1 / |\mu_2|$, the flux ratio for a power law lens becomes

$$r_{pow} = \left| \frac{\theta_1}{\theta_2} \right| \left| \frac{1 - (2-\eta)\, \theta_2^{1-\eta}\, (\theta_1 + \theta_2) \,/\, (\theta_1^{2-\eta} + \theta_2^{2-\eta})}{1 - (2-\eta)\, \theta_1^{1-\eta}\, (\theta_1 + \theta_2) \,/\, (\theta_1^{2-\eta} + \theta_2^{2-\eta})} \right|.$$

In the case of a SIS-lens, $\eta = 2$ which reduce the expression above to

$$r_{sis} = \left| \frac{\theta_1}{\theta_2} \right|.$$

F Quotient Error Propagation

Without any covariance among the observables the uncertainty becomes

$$\sigma_{q_{th}} = \left[\left(\frac{\partial q}{\partial \theta_{a_1}} \delta\theta_{a_1} \right)^2 + \left(\frac{\partial q}{\partial \theta_{a_2}} \delta\theta_{a_2} \right)^2 + \left(\frac{\partial q}{\partial \theta_{b_1}} \delta\theta_{b_1} \right)^2 + \left(\frac{\partial q}{\partial \theta_{b_2}} \delta\theta_{b_2} \right)^2 + \right.$$

$$\left. + \left(\frac{\partial q}{\partial z_a} \delta z_a \right)^2 + \left(\frac{\partial q}{\partial z_b} \delta z_b \right)^2 + \left(\frac{\partial q}{\partial z_l} \delta z_l \right)^2 \right]^{1/2}.$$

F.1 The Partial Derivative $\frac{\partial q}{\partial \theta_{a_1}}$

Let

$$A_1 = D_q \left[\theta_{b_1}^2 - \theta_{b_2}^2 \right]^{-1} \left[3 - (2-\eta)^2 \left(1 - \frac{2\,\theta_{b_2}}{\theta_{b_1} + \theta_{b_2}} \right)^2 \right]^{-1}$$

which simplifies eq. (85) as

$$q_{th} = A_1 \left[\theta_{a_1}^2 - \theta_{a_2}^2 \right] \left[3 - (2-\eta)^2 \left(1 - \frac{2\,\theta_{a_2}}{\theta_{a_1} + \theta_{a_2}} \right)^2 \right].$$

The partial derivative can then be calculated as

$$\frac{\partial q}{\partial \theta_{a_1}} = 2\,A_1 \left[3\,\theta_{a_1} - (2-\eta)^2 \left(1 - \frac{2\,\theta_{a_2}}{\theta_{a_1} + \theta_{a_2}} \right) \left(\theta_{a_1} - \frac{2\,\theta_{a_1}\theta_{a_2}}{\theta_{a_1} + \theta_{a_2}} + \frac{2\,\theta_{a_1}^2\,\theta_{a_2} - 2\,\theta_{a_2}^3}{(\theta_{a_1} + \theta_{a_2})^2} \right) \right] \iff$$

$$\iff \frac{\partial q}{\partial \theta_{a_1}} = 2A_1 \left[3\,\theta_{a_1} - (2-\eta)^2\,(\theta_{a_1} + 2\,\theta_{a_2}) \left(\frac{\theta_{a_1} - \theta_{a_2}}{\theta_{a_1} + \theta_{a_2}} \right)^2 \right].$$

F.2 The Partial Derivative $\frac{\partial q}{\partial \theta_{a_2}}$

Using the same expression for A_1 and q_{th} as above, the partial derivative can be calculated as

$$\frac{\partial q}{\partial \theta_{a_2}} = 2\,A_1 \left[-3\,\theta_{a_2} + (2-\eta)^2 \left(1 - \frac{2\,\theta_{a_2}}{\theta_{a_1} + \theta_{a_2}} \right) \left(\theta_{a_2} - \frac{2\,\theta_{a_2}^2}{\theta_{a_1} + \theta_{a_2}} + \frac{2\,\theta_{a_1}^3 - 2\,\theta_{a_1}\theta_{a_2}^2}{(\theta_{a_1} + \theta_{a_2})^2} \right) \right] \iff$$

$$\iff \frac{\partial q}{\partial \theta_{a_2}} = 2\,A_1 \left[(2-\eta)^2\,(2\,\theta_{a_1} + \theta_{a_2}) \left(\frac{\theta_{a_1} - \theta_{a_2}}{\theta_{a_1} + \theta_{a_2}} \right)^2 - 3\,\theta_{a_2} \right].$$

F.3 The Partial Derivative $\frac{\partial q}{\partial \theta_{b_1}}$

Let

$$A_2 = D_q \left[\theta_{a_1}^2 - \theta_{a_2}^2 \right] \left[3 - (2-\eta)^2 \left(1 - \frac{2\,\theta_{a_2}}{\theta_{a_1} + \theta_{a_2}} \right)^2 \right]$$

which simplifies eq. (85) as

$$q_{th} = A_2 \left[\theta_{b_1}^2 - \theta_{b_2}^2 \right]^{-1} \left[3 - (2-\eta)^2 \left(1 - \frac{2\,\theta_{b_2}}{\theta_{b_1} + \theta_{b_2}} \right)^2 \right]^{-1}.$$

Let O denote the outer derivative as

$$O = -A_2 \left[\theta_{b_1}^2 - \theta_{b_2}^2 \right]^{-2} \left[3 - (2-\eta)^2 \left(1 - \frac{2\,\theta_{b_2}}{\theta_{b_1} + \theta_{b_2}} \right)^2 \right]^{-2}.$$

The partial derivative can then be calculated as

$$\frac{\partial q}{\partial \theta_{b_1}} = 2\,O\left[3\,\theta_{b_1} - (2-\eta)^2\left(1 - \frac{2\,\theta_{b_2}}{\theta_{b_1}+\theta_{b_2}}\right)\left(\theta_{b_1} - \frac{2\,\theta_{b_1}\theta_{b_2}}{\theta_{b_1}+\theta_{b_2}} + \frac{2\,\theta_{b_2}}{(\theta_{a_1}+\theta_{a_2})^2}\,(\theta_{b_1}^2 - \theta_{b_2}^2)\right)\right] \Longleftrightarrow$$

$$\Longleftrightarrow \frac{\partial q}{\partial \theta_{b_1}} = 2\,O\left[3\,\theta_{b_1} - (2-\eta)^2\,(\theta_{b_1} + 2\,\theta_{b_2})\left(\frac{\theta_{b_1}-\theta_{b_2}}{\theta_{b_1}+\theta_{b_2}}\right)^2\right].$$

F.4 The Partial Derivative $\frac{\partial q}{\partial \theta_{b_2}}$

Using the same expression for O and q_{th} as above, the partial derivative can be calculated as

$$\frac{\partial q}{\partial \theta_{b_2}} = 2\,O\left[-3\theta_{b_2} + (2-\eta)^2\left(1 - \frac{2\,\theta_{b_2}}{\theta_{b_1}+\theta_{b_2}}\right)\left(\theta_{b_2} - \frac{2\,\theta_{b_2}^2}{\theta_{b_1}+\theta_{b_2}} + \frac{2\,\theta_{b_1}}{(\theta_{b_1}+\theta_{b_2})^2}\,(\theta_{b_1}^2 - \theta_{b_2}^2)\right)\right] \Longleftrightarrow$$

$$\Longleftrightarrow \frac{\partial q}{\partial \theta_{b_2}} = 2\,O\left[(2-\eta)^2\,(2\,\theta_{b_1} + \theta_{b_2})\left(\frac{\theta_{b_1}-\theta_{b_2}}{\theta_{b_1}+\theta_{b_2}}\right)^2 - 3\,\theta_{b_2}\right].$$

F.5 The Partial Derivative $\frac{\partial q}{\partial z_i}$

Equation (87) gives that angular distance quotient can be written as

$$D_q = \frac{d_a\left(d_b - d_l\right)}{d_b\left(d_a - d_l\right)}$$

where

$$d_i = \int_{z_0}^{z_i} \frac{d\acute{z}}{\left[\Omega_M(\,(1+\acute{z})^3 - 1) + 1\right]^{1/2}}.$$

Let

$$A_3 = \left[\frac{\theta_{a_1}^2 - \theta_{a_2}^2}{\theta_{b_1}^2 - \theta_{b_2}^2}\right]\left[\frac{3 - (2-\eta)^2\left(1 - \frac{2\theta_{a_2}}{\theta_{a_1}+\theta_{a_2}}\right)^2}{3 - (2-\eta)^2\left(1 - \frac{2\theta_{b_2}}{\theta_{b_1}+\theta_{b_2}}\right)^2}\right].$$

Taking the partial derivative for every redshift gives then

$$\frac{\partial q}{\partial z_a} = A_3\,\frac{d_a'\,d_l\,(d_l - d_b)}{d_b\,(d_a - d_l)^2},$$

$$\frac{\partial q}{\partial z_b} = A_3\,\frac{d_b'\,d_a\,d_l}{d_b^2\,(d_a - d_l)},$$

$$\frac{\partial q}{\partial z_l} = A_3\,\frac{d_l'\,d_a\,(d_b - d_a)}{d_b\,(d_a - d_l)^2},$$

where

$$d_i' = \left[\Omega_M(\,(1+\acute{z})^3 - 1) + 1\right]^{-1/2}$$

F.6 The Uncertainty σ_{th}

The uncertainty can now be written as

$$\sigma_{th} = 2\,D_q\left[\theta_{b_1}^2-\theta_{b_2}^2\right]^{-1}\left[3-(2-\eta)^2\left(1-\frac{2\,\theta_{b_2}}{\theta_{b_1}+\theta_{b_2}}\right)^2\right]^{-1}\Bigg\{\Bigg[3\,\theta_{a_1}-(2-\eta)^2\,(\theta_{a_1}+2\,\theta_{a_2})\cdots$$

$$\cdots\left(\frac{\theta_{a_1}-\theta_{a_2}}{\theta_{a_1}+\theta_{a_2}}\right)^2\Bigg]^2\delta\theta_{a_1}^2+\left[(2-\eta)^2\,(2\,\theta_{a_1}+\theta_{a_2})\left(\frac{\theta_{a_1}-\theta_{a_2}}{\theta_{a_1}+\theta_{a_2}}\right)^2-3\,\theta_{a_2}\right]^2\delta\theta_{a_2}^2+$$

$$+\left[\frac{\theta_{a_1}^2-\theta_{a_2}^2}{\theta_{b_1}^2-\theta_{b_2}^2}\right]^2\left[\frac{3-(2-\eta)^2\left(1-\frac{2\theta_{a_2}}{\theta_{a_1}+\theta_{a_2}}\right)^2}{3-(2-\eta)^2\left(1-\frac{2\theta_{b_2}}{\theta_{b_1}+\theta_{b_2}}\right)^2}\right]^2\Bigg[\Bigg[3\,\theta_{b_1}-(2-\eta)^2\,(\theta_{b_1}+2\,\theta_{b_2})\cdots$$

$$\cdots\left(\frac{\theta_{b_1}-\theta_{b_2}}{\theta_{b_1}+\theta_{b_2}}\right)^2\Bigg]^2\delta\theta_{b_1}^2+\left[3\,\theta_{b_1}-(2-\eta)^2\,(\theta_{b_1}+2\,\theta_{b_2})\left(\frac{\theta_{b_1}-\theta_{b_2}}{\theta_{b_1}+\theta_{b_2}}\right)^2\right]^2\delta\theta_{b_2}^2\Bigg]+\left[\frac{\theta_{a_1}^2-\theta_{a_2}^2}{2\,D_q}\right]^2\cdots$$

$$\cdots\left[3-(2-\eta)^2\left(1-\frac{2\theta_{a_2}}{\theta_{a_1}+\theta_{a_2}}\right)^2\right]^2\left[\frac{1}{d_b^2\,(d_a-d_l)^2}\right]^2\Bigg[\left(\frac{d_a'\,d_l\,(d_l-d_b)}{(d_a-d_l)}\,\delta z_a\right)^2+$$

$$\left(\frac{d_b'\,d_a\,d_l}{d_b}\,\delta z_b\right)^2+\left(\frac{d_l'\,d_a\,(d_b-d_a)}{(d_a-d_l)}\,\delta z_l\right)^2\Bigg]\Bigg\}^{1/2}.$$

G Summing χ^2 Error Propagation

Without any covariance, eq. (70) gives the uncertainties propagating as

$$\sigma_{i_{t\,h}} = \left[\left(\frac{\partial \Delta t}{\partial \theta_{i1}} \, \delta\theta_{i1} \right)^2 + \left(\frac{\partial \Delta t}{\partial \theta_{i2}} \, \delta\theta_{i2} \right)^2 + \left(\frac{\partial \Delta t}{\partial z_i} \, \delta z_i \right)^2 + \left(\frac{\partial \Delta t}{\partial z_l} \, \delta z_l \right)^2 + \left(\frac{\partial \Delta t}{\partial P} \, \delta P \right)^2 \right]^{1/2}.$$

G.1 The Partial Derivative $\frac{\partial \Delta t}{\partial \theta_{i1}}$

Let

$$A_1 = \frac{1}{2} \left[\frac{1 + z_l}{c} \right] \left[\frac{D_l \, D_i}{D_{li}} \right] (\eta - 1)$$

which simplifies eq. (70) as

$$\Delta t = A_1 \left(\theta_{i1}^2 - \theta_{i2}^2 \right) \left[1 - \frac{(2-\eta)^2}{3} \left(1 - \frac{2\,\theta_{i2}}{\theta_{i1} + \theta_{i2}} \right)^2 \right].$$

The partial derivative can then be calculated as

$$\frac{\partial \Delta t}{\partial \theta_{i1}} = 2\,A_1 \left[\theta_{i1} - \frac{(2-\eta)^2}{3} \left(1 - \frac{2\,\theta_{i2}}{\theta_{i1} + \theta_{i2}} \right) \left[\theta_{i1} - \frac{2\,\theta_{i1}\theta_{i2}}{\theta_{i1} + \theta_{i2}} + \frac{2\,\theta_{i2}}{\left(\theta_{i1} + \theta_{i2} \right)^2} \left(\theta_{i1}^2 - \theta_{i2}^2 \right) \right] \right] \iff$$

$$\iff \frac{\partial \Delta t}{\partial \theta_{i1}} = 2\,A_1 \left[\theta_{i1} - \frac{(2-\eta)^2}{3} \left(\theta_{i1} + 2\,\theta_{i2} \right) \left(\frac{\theta_{i1} - \theta_{i2}}{\theta_{i1} + \theta_{i2}} \right)^2 \right]$$

G.2 The Partial Derivative $\frac{\partial \Delta t}{\partial \theta_{i2}}$

Using the same expression for A_1 and Δt as above, the partial derivative can be calculated as

$$\frac{\partial \Delta t}{\partial \theta_{i2}} = 2\,A_1 \left[-\theta_{i2} + \frac{(2-\eta)^2}{3} \left(1 - \frac{2\,\theta_{i2}}{\theta_{i1} + \theta_{i2}} \right) \left[\theta_{i2} - \frac{2\,\theta_{i2}^2}{\theta_{i1} + \theta_{i2}} + \frac{2\,\theta_{i1}}{\left(\theta_{i1} + \theta_{i2} \right)^2} \left(\theta_{i1}^2 - \theta_{i2}^2 \right) \right] \right] \iff$$

$$\iff \frac{\partial \Delta t}{\partial \theta_{i2}} = 2\,A_1 \left[\frac{(2-\eta)^2}{3} \left(2\,\theta_{i1} + \theta_{i2} \right) \left(\frac{\theta_{i1} - \theta_{i2}}{\theta_{i1} + \theta_{i2}} \right)^2 - \theta_{i2} \right].$$

G.3 The Partial Derivatives $\frac{\partial \Delta t}{\partial z_i}$ and $\frac{\partial \Delta t}{\partial z_l}$

Let

$$A_2 = \frac{1}{2\,c} \, (\eta - 1) \left(\theta_{i1}^2 - \theta_{i2}^2 \right) \left[1 - \frac{(2-\eta)^2}{3} \left(1 - \frac{2\,\theta_{i2}}{\theta_{i1} + \theta_{i2}} \right)^2 \right] \quad \text{, and} \quad D = \left[\frac{D_l \, D_i}{D_{li}} \right]$$

which simplifies eq. (70) as

$$\Delta t = A_2 \, (1 + z_l) \, D.$$

Equation (35) gives

$$D = \frac{\frac{c}{H_0\,(1+z_l)} \int_{z_0}^{z_l} \frac{d\acute{z}}{[\Omega_M((1+\acute{z})^3 - 1) + 1]^{1/2}} \cdot \frac{c}{H_0\,(1+z_i)} \int_{z_0}^{z_i} \frac{d\acute{z}}{[\Omega_M((1+\acute{z})^3 - 1) + 1]^{1/2}}}{\frac{c}{H_0\,(1+z_i)} \left[\int_{z_0}^{z_i} \frac{d\acute{z}}{[\Omega_M((1+\acute{z})^3 - 1) + 1]^{1/2}} - \int_{z_0}^{z_l} \frac{d\acute{z}}{[\Omega_M((1+\acute{z})^3 - 1) + 1]^{1/2}} \right]} \implies$$

$$\implies \Delta t = A_2 \, \frac{c}{H_0} \, \frac{\int_{z_0}^{z_l} \frac{d\acute{z}}{[\Omega_M((1+\acute{z})^3 - 1) + 1]^{1/2}} \int_{z_0}^{z_i} \frac{d\acute{z}}{[\Omega_M((1+\acute{z})^3 - 1) + 1]^{1/2}}}{\left[\int_{z_0}^{z_i} \frac{d\acute{z}}{[\Omega_M((1+\acute{z})^3 - 1) + 1]^{1/2}} - \int_{z_0}^{z_l} \frac{d\acute{z}}{[\Omega_M((1+\acute{z})^3 - 1) + 1]^{1/2}} \right]}.$$

By setting

$$d = \int_{z_0}^{z} \frac{d\acute{z}}{\left[\Omega_M\left((1+\acute{z})^3 - 1\right) + 1\right]^{1/2}} \quad \text{, and} \quad d' = \left[\Omega_M\left((1+\acute{z})^3 - 1\right) + 1\right]^{-1/2},$$

the partial derivatives can then be calculated as

$$\frac{\partial \Delta t}{\partial z_i} = A_2 \, \frac{c}{H_0} \left[- \frac{d_i' \, d_l^2}{(d_i - d_l)^2} \right],$$

$$\frac{\partial \Delta t}{\partial z_l} = A_2 \, \frac{c}{H_0} \left[\frac{d_l' \, d_i^2}{(d_i - d_l)^2} \right].$$

G.4 The Partial Derivative $\frac{\partial \Delta t}{\partial \eta}$

Let

$$A_4 = \frac{1}{2} \left[\frac{1 + z_l}{c} \right] \left[\frac{D_l \, D_i}{D_{li}} \right] \left(\theta_{i1}^2 - \theta_{i2}^2 \right)$$

which simplifies eq. (70) as

$$\Delta t = A_4 \, (\eta - 1) \left[1 - \frac{(2-\eta)^2}{3} \left(1 - \frac{2\,\theta_{i2}}{\theta_{i1} + \theta_{i2}} \right)^2 \right].$$

The partial derivative can then be calculated as

$$\frac{\partial \Delta t}{\partial \eta} = A_4 \left[1 + \frac{(2-\eta)}{3} \left(1 - \frac{2\,\theta_{i2}}{\theta_{i1} + \theta_{i2}} \right)^2 \left(2\left(\eta - 1\right) - \left(2 - \eta\right) \right) \right] \iff$$

$$\iff \frac{\partial \Delta t}{\partial \eta} = A_4 \left[1 + \frac{(2-\eta)}{3} \left(1 - \frac{2\,\theta_{i2}}{\theta_{i1} + \theta_{i2}} \right)^2 \left(3\,\eta - 4 \right) \right].$$

G.5 The Uncertainty $\sigma_{i_{th}}$

The uncertainty can now be written as

$$\sigma_{i_{th}} = \frac{1}{2} \, (\eta - 1) \Bigg\{ \left(\theta_{i1}^2 - \theta_{i2}^2 \right)^2 \left[1 - \frac{(2-\eta)^2}{3} \left(1 - \frac{2\,\theta_{i2}}{\theta_{i1} + \theta_{i2}} \right)^2 \right]^2 \frac{1}{H_0^2 \, (d_i - d_l)^4} \left[\left(d_i' \, d_l^2 \, \delta z_i \right)^2 + \right.$$

$$\left(d_l' \, d_i^2 \, \delta z_l \right)^2 \Big] + \frac{4}{H_0^2} \left[\frac{d_l \, d_i}{d_{li}} \right]^2 \Bigg[\left(\theta_{i1} - \frac{(2-\eta)^2}{3} \left(\theta_{i1} + 2\,\theta_{i2} \right) \left(\frac{\theta_{i1} - \theta_{i2}}{\theta_{i1} + \theta_{i2}} \right)^2 \right)^2 \delta_{\theta_{i1}}^2 +$$

$$\left. \left(\frac{(2-\eta)^2}{3} \left(2\,\theta_{i1} + \theta_{i2} \right) \left(\frac{\theta_{i1} - \theta_{i2}}{\theta_{i1} + \theta_{i2}} \right)^2 - \theta_{i2} \right)^2 \delta_{\theta_{i2}}^2 \Bigg] \right\}^{1/2}.$$